On loading paths followed inside plastic simple waves in two-dimensional elastic-plastic solids

Adrien Renaud, Thomas Heuzé, Laurent Stainier

On loading paths followed inside plastic simple waves in two-dimensional elastic-plastic solids

Adrien Renaud[1,2], Thomas Heuzé[2], Laurent Stainier[2]

[1] *Laboratory MSSMat (UMR 8579 CNRS)*
CentraleSupélec, Université Paris-Saclay
8-10 rue Joliot-Curie, 91190 Gif-sur-Yvette
e-mail: adrien.renaud@centralesupelec.fr

[2] *Research Institute in Civil and Mechanical Engineering (GeM, UMR 6183 CNRS)*
Ecole Centrale de Nantes
1 rue de la Noë, Nantes
e-mail: {thomas.heuze,laurent.stainier}@ec-nantes.fr

Abstract

Although the solution of hyperbolic partial differential equations in elastic-plastic media is of major importance in solid mechanics, the mathematical complexity of such problems increases with the space dimensionality. As a result, the development of analytical solutions is in general not possible. Whereas the wave structure resulting from given external loads is known and well understood for one-dimensional problems, several gaps still need to be filled for problems with more space dimensions. Indeed, the literature related to the propagation of simple waves in elastic-plastic solids is rather sparse since only particular two-dimensional and three-dimensional problems have been considered. Following the general three-dimensional framework of Mandel (1962), the object of the paper is to construct the loading paths followed inside the simple waves under plane strain and plane stress conditions. It is believed that the mathematical and numerical studies of the waves presented here could help define the characteristic structure involved in a Riemann problem.

Keywords: Hyperbolic problems; Elastic-plastic solids; Simple waves; Loading paths; Characteristic analysis.

1. Introduction

A wide variety of engineering problems including acoustics, aerodynamics or impacts, are modeled with hyperbolic systems of conservation laws. Applications such as high-speed metal forming techniques or crash-proof design moreover involve elastic-plastic solids, whose response depends on history effects. The irreversible deformations occurring in this class of solids, which are related to the evolution of the microstructure of the material, are of primary importance to finally access to residual strains and stresses. Therefore, the waves arising in the solutions of hyperbolic systems in elastic-plastic materials, as well as their interactions with each other, must be precisely followed so that the sequence of propagated states can be connected to residual states.

Even though calculating the exact solutions of this class of problems is in general not possible for elastic-plastic media, they are known in particular cases. Until the 50s, research on dynamic problems in those solids were focused on uni-axial stress or strain, pure bending or pure torsion loading conditions [1, 2], and were carried out for material characterization purposes. Then, Rakhmatulin [3] and Cristescu [4] investigated the response of linearly hardening solids to combined shear and pressure dynamic loads. These early works on plane stress impacts in the plastic regime led to the conclusion that elastic waves, as well as plastic combined-stress simple waves, can propagate in two-dimensional solids. While the former were well-known, the latter were shown to fall into two families: the *fast waves* and the *slow waves*. The analysis of the solution to general three-dimensional problems by Mandel [5] and Hill [6] confirmed the existence of those families by providing a complete characterization of the wave speeds and the formulation of the jump conditions across the elastic-plastic boundaries.

Later, Bleich and Nelson [7] considered superimposed plane and shear waves in an ideally elastic-plastic material submitted to step loads. It has then been highlighted that different loading cases yield different characteristic structures of the solution in problems defined in a semi-infinite medium with prescribed traction forces and initial conditions (the so-called Picard problem). The results of Bleich and Nelson thus revealed the complexity of plastic flows in multi-dimensional solids undergoing dynamic loadings. The same conclusions have been drawn by Clifton [8] for hardening materials under tension-torsion, who furthermore studied the influence of plastic pre-loading on the solution. This contribution highlighted the combined-stress wave nature lying in Ordinary Differential Equations (ODEs) that arise from the characteristic analysis of the hyperbolic system and govern the evolution of stress components within the simple waves. The integration of these equations allows the building of curves that connect the applied stress state in the Picard problem to the initial state of the medium. It has been for instance shown that if a solid is acted upon by a pure shear traction beyond the elastic domain, only an elastic shear discontinuity, followed by a slow simple wave, propagates. Conversely, other loading conditions may lead to the combination of an elastic pressure discontinuity and a fast wave, possibly followed by a slow wave. Another notable conclusion is that the loading paths followed inside plastic simple waves are not necessarily radial even if a von-Mises flow rule is considered. Experimental data collected on a thin-walled tube submitted to a dynamic tensile load [9, 10] confirmed the existence of two distinct families of simple waves, both involving combined stress paths. Ting and Nan [11] then generalized the work of Bleich and Nelson to hardening materials and Ting [12] widened that of Clifton to more complex loadings, that is, a superimposition of one plane wave and two shear waves. Once again, the mathematical study of the ODE system governing the stress evolution inside fast and slow simple waves led to the construction of loading paths in the stress space. A review of the governing equations for all the cases depending on one space dimension considered above can be found in [13].

Besides the above works on the simple wave solutions, several authors studied the existence of plastic shocks in solids under plane wave assumptions [5, 14, 15, 16, 17, 18, 19]. These references nevertheless consider hydro-elastic-plastic solids for which the hydrostatic part of the behavior follows some particular convex state law for the pressure, which can lead to plastic shock solutions. On the contrary, provided a classical Hooke elastic compressibility, only plastic simple waves can occur in the solution of Picard problems.

Research conducted on plastic waves enable the derivation of exact solutions for problems with simple geometries and loadings. For more complex problems however, approximate solutions can be computed through the use of numerical approaches. In particular, the family of Godunov's methods [20] allows to take into account the characteristic structure of the solution of hyperbolic problems so as to accurately capture waves. These methods are based on the solution of a Riemann problem whose construction requires to know the wave pattern *a priori*, which is not possible for elastic-plastic solids. For the thin-walled tube problem, Lin and Ballman overtook this difficulty by defining elementary stress paths from Clifton's results [21]. Those paths can be used in order to relate some guessed stationary state of the Riemann problem to its initial conditions through the waves involved and hence to deduce the wave pattern. By iteratively following that procedure until convergence, the Riemann problem can be solved.

The purpose of the present work is the determination of the loading paths followed inside the plastic simple waves involved in two-dimensional elastic-plastic media. This contribution can therefore be seen as an extension of the work of Clifton [8] to more general two-dimensional problems in order to deduce loading paths from the characteristic structure of the hyperbolic system. As we shall see, the stress states considered lead to paths that are very different from those observed in one-dimensional problems. The long-term goal of that research is the extension to general two-dimensional problems of the approach of Lin and Ballman.

In what follows, the characteristic analysis of the governing equations of dynamics in elastic-plastic solids is carried out and some important results of Mandel [5] are recalled in section 2. Then, the equations are particularized to two-dimensional problems so that the method of characteristics is applied in section 4 in order to derive the equations of integral curves. Those curves, once projected into the stress space, correspond to the loading paths that have been already identified for other problems. Section 5 is devoted to the mathematical properties of the aforementioned loading paths which, given the complexity of the equations, is supplemented with numerical results presented in section 6.

2. Hyperbolic system in elastic-plastic media

In this section, the governing equations of general dynamic problems in elastic-plastic solids are first written with a tensorial formalism based on the fourth-order stiffness tensor. This framework leads on the one hand to the same characteristic structure as in [22, 23], so that well known results can be used. On the other hand, it allows easy specialization to problems involving less than three space dimensions, such as the one-dimensional ones already treated in the literature. Second, the spectral analysis of the hyperbolic system written in an arbitrary direction is performed, which is motivated by the solution of Riemann problems in one space dimension in numerical schemes such as the Finite Volume Method (FVM) [24, 25]. That approach furthermore avoids the seeking of bi-characteristics as proposed by Clifton in order to build elastoplastic finite difference schemes [26]. It must be emphasized that the present work aims at highlighting a sufficient amount of information so as to enable numerical schemes to mimic the analytical behavior, and does not require the complete bi-characteristic structure.

2.1. Governing equations

We consider the isothermal deformation of a solid body of mass density ρ in the linearized geometrical framework. The balance equation of linear momentum with neglected body forces, and the geometrical balance equations [27, 28] are:

$$\begin{aligned} &\rho\dot{\boldsymbol{v}} - \boldsymbol{\nabla}\cdot\boldsymbol{\sigma} = \boldsymbol{0} \\ &\dot{\boldsymbol{\varepsilon}} - \boldsymbol{\nabla}\cdot\left(\frac{\boldsymbol{v}\otimes\boldsymbol{I} + \boldsymbol{I}\boxtimes\boldsymbol{v}}{2}\right) = \boldsymbol{0} \end{aligned} \tag{1}$$

where the operator $\boxtimes$ refers to the transpose on second and third indices of the classical tensor product, namely: $\boldsymbol{I}\boxtimes\boldsymbol{v} = \delta_{ik}v_j\boldsymbol{e}_i\otimes\boldsymbol{e}_j\otimes\boldsymbol{e}_k$. Furthermore, $\boldsymbol{I}$, $\boldsymbol{v}$, $\boldsymbol{\sigma}$ and $\boldsymbol{\varepsilon}$ denote respectively the second-order identity tensor, the velocity vector, the Cauchy stress tensor and the linearized strain tensor. The latter additively decomposes into an elastic strain $\boldsymbol{\varepsilon}^e$ and a plastic strain $\boldsymbol{\varepsilon}^p$ in the small strain case. Assuming Cartesian coordinates, system (1) can be written as:

$$\frac{\partial\mathcal{U}}{\partial t} + \frac{\partial\mathcal{F}\cdot\boldsymbol{e}_i}{\partial x_i} = \boldsymbol{0} \tag{2}$$

with the vector of conserved quantities $\mathcal{U}$ and the flux vectors $\mathcal{F}_i = \mathcal{F}\cdot\boldsymbol{e}_i$:

$$\mathcal{U} = \begin{bmatrix}\rho\boldsymbol{v}\\ \boldsymbol{\varepsilon}\end{bmatrix} \quad ; \quad \mathcal{F}_i = \begin{bmatrix}-\boldsymbol{\sigma}\cdot\boldsymbol{e}_i\\ -\frac{\boldsymbol{v}\otimes\boldsymbol{e}_i+\boldsymbol{e}_i\otimes\boldsymbol{v}}{2}\end{bmatrix}$$

Alternatively, the introduction of an auxiliary vector of conserved quantities $\mathcal{Q}$ allows rewriting equation (2) as a quasi-linear form by means of the chain rule [29]:

$$\frac{\partial\mathcal{Q}}{\partial t} + \mathbf{A}^i\frac{\partial\mathcal{Q}}{\partial x_i} = \boldsymbol{0} \tag{3}$$

In particular, by setting $\mathcal{Q} = \begin{bmatrix}\boldsymbol{v}\\ \boldsymbol{\sigma}\end{bmatrix}$, one writes:

$$\mathbf{A}^i = \left(\frac{\partial\mathcal{U}}{\partial\mathcal{Q}}\right)^{-1}\frac{\partial\mathcal{F}_i}{\partial\mathcal{Q}} = -\begin{bmatrix}\boldsymbol{0}^2 & \frac{1}{\rho}\left(\frac{\boldsymbol{I}\otimes\boldsymbol{e}_i+\boldsymbol{e}_i\otimes\boldsymbol{I}}{2}\right)\\ \mathbb{H}\cdot\boldsymbol{e}_i & \boldsymbol{0}^4\end{bmatrix},$$

$\boldsymbol{0}^q$ being a qth-order zero tensor and $\mathbb{H} = \frac{\partial\boldsymbol{\sigma}}{\partial\boldsymbol{\varepsilon}}$ the fourth-order tangent modulus tensor. It then appears that the characteristic structure of the hyperbolic problem, which is driven by the matrices $\mathbf{A}^i$, depends on the nature of the deformation (*i.e. elastic or elastic-plastic*) through the tangent modulus.

Following the Generalized Standard Material framework [30], the elastic-plastic constitutive response is described by a Helmholtz free-energy ψ, convex with respect to $\boldsymbol{\varepsilon}$ and the set of additional internal variables $\mathcal{V}$, and a yield surface f in the case of associative plasticity. Assuming elastic isotropy, reversible evolutions are governed by the elastic law derived from Helmholtz's free energy:

$$\boldsymbol{\sigma} = \mathbb{C} : \boldsymbol{\varepsilon}^e = 2\mu\boldsymbol{\varepsilon}^e + \lambda\,\mathrm{trace}\;\boldsymbol{\varepsilon}^e\,\boldsymbol{I} \tag{4}$$

in which (λ, μ) are Lamé's parameters. The inverse constitutive law can also be written based on Young's modulus and Poisson's ratio (E, ν):

$$\boldsymbol{\varepsilon}^e = \mathbb{C}^{-1} : \boldsymbol{\sigma} = \frac{1+\nu}{E}\boldsymbol{\sigma} - \frac{\nu}{E}\,\text{trace}\;\boldsymbol{\sigma}\,\boldsymbol{I} \tag{5}$$

Next, restricting ourselves to isotropic hardening, the set $\boldsymbol{\mathcal{V}}$ consists of the cumulated plastic strain p. In addition, the von-Mises yield surface is considered:

$$f(\boldsymbol{\sigma}, R) = \sqrt{\frac{3}{2}}\,\|\boldsymbol{s}\| - (R(p) + \sigma^y) \leq 0 \tag{6}$$

where $\boldsymbol{s}$ denotes the deviatoric part of the Cauchy stress tensor, σ^y is the yield stress in tension, and $-R(p)$ is the thermodynamical force conjugate to the cumulated plastic strain through some hardening law. The evolution of the plastic strain tensor and the cumulated plastic strain are governed by the following flow rule and hardening law respectively:

$$\dot{\boldsymbol{\varepsilon}}^p = \lambda\frac{\partial f}{\partial \boldsymbol{\sigma}} \tag{7}$$

$$\dot{p} = -\lambda\frac{\partial f}{\partial R} \tag{8}$$

where the plastic multiplier λ and the yield surface obey the Kuhn-Tucker complementarity conditions:

$$\lambda \geq 0 \quad ; \quad f \leq 0 \quad ; \quad \lambda f = 0$$

along with the consistency condition:

$$\lambda \dot{f} = 0$$

Therefore, combining equations (7) and (8), the flow rule can be rewritten as:

$$\dot{\boldsymbol{\varepsilon}}^p = \dot{p}\,\sqrt{\frac{3}{2}}\frac{\boldsymbol{s}}{\|\boldsymbol{s}\|} \tag{9}$$

Given this description of internal processes, the thermodynamical framework then leads to the elastic-plastic constitutive equations during irreversible deformations by combining the elastic law (4), the additive decomposition of the strain tensor and the plastic flow rule (9) [31]:

$$\dot{\boldsymbol{\sigma}} = \mathbb{C}^{ep} : \dot{\boldsymbol{\varepsilon}} = (\mathbb{C} - \beta\,\boldsymbol{s}\otimes\boldsymbol{s}) : \dot{\boldsymbol{\varepsilon}} \tag{10}$$

$$\beta = \frac{6\mu^2}{3\mu + R'} \times \frac{1}{\boldsymbol{s} : \boldsymbol{s}}$$

where the elastoplastic tangent modulus $\mathbb{C}^{ep}$ can be decomposed into the elasticity tensor $\mathbb{C}$ and another part depending on the direction of the plastic flow. Therefore, plastic evolutions involve $\mathbb{H} \equiv \mathbb{C}^{ep}$ while elastic ones involve $\mathbb{H} \equiv \mathbb{C}$.

2.2. Spectral analysis

Considering an arbitrary direction of space $\boldsymbol{n}$, the quasi-linear form (3) reads:

$$\frac{\partial \boldsymbol{\mathcal{Q}}}{\partial t} + \mathbf{J}\frac{\partial \boldsymbol{\mathcal{Q}}}{\partial x_n} = \mathbf{0} \tag{11}$$

where $x_n = \boldsymbol{x}\cdot\boldsymbol{n}$ and $\mathbf{J} = n_i\mathbf{A}^i$ is the Jacobian matrix. Simple waves are solutions for which the vector $\boldsymbol{\mathcal{Q}}$ is constant along each curve of the one-parameter family $\eta^K(x_n, t) = \text{const}$. For such *self-similar* solutions, system (11) reads:

$$\left(\mathbf{J} - c_K\mathbf{I}\right)\boldsymbol{\mathcal{Q}}'(\eta^K) = \mathbf{0} \tag{12}$$

where $\mathbf{I}$ is the 9×9 identity matrix and $c_K = -\frac{\partial \eta^K}{\partial t} / \frac{\partial \eta^K}{\partial x_n}$ appears to be the Kth eigenvalue of the Jacobian matrix. The problem therefore admits nontrivial solutions if $\mathbf{J}$ has real eigenvalues and distinct left eigenvectors $\mathcal{L}^K = \left[\boldsymbol{v}^K \,,\, \boldsymbol{\sigma}^K\right]$ satisfying:

$$\mathcal{L}^K \left(\mathbf{J} - c_K \mathbf{I}\right) = \mathbf{0} \qquad K = 1, \cdots, 9$$

Thus, for non-zero eigenvalues one gets:

$$-\boldsymbol{\sigma}^K : (\mathbb{H} \cdot \boldsymbol{n}) - c_K \boldsymbol{v}^K = \mathbf{0} \tag{13}$$

$$-\frac{1}{\rho} \boldsymbol{v}^K \otimes \boldsymbol{n} - c_K \boldsymbol{\sigma}^K = \mathbf{0} \tag{14}$$

Substitution of $\boldsymbol{\sigma}^K$ obtained from (14) in (13) leads to:

$$(\boldsymbol{v}^K \otimes \boldsymbol{n}) : (\mathbb{H} \cdot \boldsymbol{n}) - \rho c_K^2 \boldsymbol{v}^K = \mathbf{0} \tag{15}$$

which is the left eigensystem of the acoustic tensor $A_{ij} = n_k H_{ikjl} n_l$. Due to the symmetry of $\boldsymbol{A}$, system (15) is equivalent to the right eigensystem:

$$\left(n_k H_{ikjl} n_l - \rho c_K^2 \delta_{ij}\right) v_j^K = 0$$

or alternatively, with the eigenvalues ω_p and associated left eigenvectors of the acoustic tensor $\boldsymbol{l}^q$ $(q = 1, 2, 3)$:

$$\boldsymbol{l}^q \cdot \left(\boldsymbol{A} - \omega_q \boldsymbol{I}\right) = \mathbf{0} \tag{16}$$

The condition for system (11) to be hyperbolic (real eigenvalues and independent eigenvectors) is thus ensured by the positive definiteness of the acoustic tensor, also known as the *strong ellipticity* condition [32]:

$$(\boldsymbol{m} \otimes \boldsymbol{n}) : \mathbb{H} : (\boldsymbol{n} \otimes \boldsymbol{m}) > 0 \quad \forall \boldsymbol{n}, \boldsymbol{m} \in \mathbb{R}^3 \,;\, \boldsymbol{n}, \boldsymbol{m} \neq \mathbf{0}$$

If the condition holds, the acoustic tensor admits 3 couples of eigenvalue–eigenvector $\{\omega_q, \boldsymbol{l}^q\}$ leading to 6 couples $\{c_K, \mathcal{L}^K\}$ for the Jacobian matrix, the 3 other eigenvalues being null [33]. The couples $\{c_K, \mathcal{L}^K\}$ are referred to as the *left characteristic fields*. Notice that since the elastic stiffness tensor $\mathbb{C}$ or the elastoplastic tangent modulus $\mathbb{C}^{ep}$ may be involved in equation (3), three left characteristic fields are obviously associated with elastic and elastic-plastic evolutions respectively. The left eigenvectors related to the non-zero eigenvalues of the Jacobian matrix are obtained by using equation (14) so that the following 6 eigenfields of the quasi-linear form (11) can be defined:

$$\left\{ \pm \sqrt{\frac{\omega_q}{\rho_0}}; \left[\pm \rho_0 \sqrt{\frac{\omega_q}{\rho_0}} \boldsymbol{l}^q, -\boldsymbol{l}^q \otimes \boldsymbol{n} \right] \right\}, \; q = 1, 2, 3 \tag{17}$$

At last, three independent left eigenvectors associated with the null eigenvalue of multiplicity 3 can be found by solving equation (13) for the null eigenvalue:

$$\boldsymbol{\sigma}^K : (\mathbb{H} \cdot \boldsymbol{n}) = \mathbf{0}, \quad K = 1, ..., 3 \tag{18}$$

Since the above formulation is based on the elastoplastic stiffnesses rather than compliances, it differs from those of Bleich [7], Clifton [8], and hence from these of Ting and Nan [11] and Ting [12]. The use of the tangent modulus $\mathbb{H}$ enables the specialization of equations (17) and (18) to the plane strain and the plane stress cases, as we shall see in section 3.

2.3. Known properties of the plastic waves

Let us now recall some of the important results of Mandel [5, 34] for which proofs can also be found in [23]. Denoting the elastic acoustic tensor as $\boldsymbol{A}^e = \boldsymbol{n} \cdot \mathbb{C} \cdot \boldsymbol{n}$, the eigenvalue problem (16) can be rewritten as:

$$\boldsymbol{l}^q \cdot (\boldsymbol{B} - \beta \boldsymbol{a} \otimes \boldsymbol{a}) = \mathbf{0} \tag{19}$$

in which $\boldsymbol{B} = \boldsymbol{A}^e - \omega_q \boldsymbol{I}$ and $\boldsymbol{a} = \boldsymbol{s} \cdot \boldsymbol{n}$. Then, assuming that the coordinate axes coincide with the eigenbasis of $\boldsymbol{A}^e$, the determinant of system (19) reads:

$$F(\omega_q) = (A_1^e - \omega_q)(A_2^e - \omega_q)(A_3^e - \omega_q) - \beta \left[(A_2^e - \omega_q)(A_3^e - \omega_q) a_1^2 + (A_1^e - \omega_q)(A_3^e - \omega_q) a_2^2 + (A_1^e - \omega_q)(A_2^e - \omega_q) a_3^2 \right] = 0$$

With $\beta > 0$ and the eigenvalues of $\boldsymbol{A^e}$ satisfying $A_1^e \geq A_2^e \geq A_3^e$, it comes out that:

$$F\left(A_1^e\right) \leq 0 \quad ; \quad F\left(A_2^e\right) \geq 0 \quad ; \quad F(A_3^e) \leq 0 \quad ; \quad F(\infty) < 0$$

from which the following conclusion is drawn.

Property 1 (First Mandel's inequality). *For a unit normal vector $\boldsymbol{n}$, the speeds of plastic waves $c_I^p \geq c_{II}^p \geq c_{III}^p$ are bounded by the elastic speeds $c_I^e \geq c_{II}^e \geq c_{III}^e$ according to:*

$$c_I^e \geq c_I^p \geq c_{II}^e \geq c_{II}^p \geq c_{III}^e \geq c_{III}^p$$

Consider now equation (12), from which one gets for plastic evolutions:

$$\boldsymbol{\sigma}' = -\frac{1}{c_K} \mathbb{H} : (\boldsymbol{n} \otimes \boldsymbol{v}') \tag{20}$$

$$\left(\boldsymbol{A}^{ep} - \rho c_K^2 \boldsymbol{I} \right) \boldsymbol{v}' = \boldsymbol{0} \tag{21}$$

If one of the plastic speed is equal to an elastic speed, the expansion of equation (21) leads to:

$$\beta \boldsymbol{a} \cdot \boldsymbol{v}' = 0 \tag{22}$$

Then, the projection of the variation $\boldsymbol{\sigma}'$ from equation (20) onto the normal to the yield surface is:

$$\frac{\partial f}{\partial \boldsymbol{\sigma}} : \boldsymbol{\sigma}' = \frac{1}{c_K} \sqrt{\frac{3}{2}} \frac{\mu - \beta \|\boldsymbol{s}\|}{\|\boldsymbol{s}\|} \boldsymbol{a} \cdot \boldsymbol{v}' = 0$$

Hence, if condition (22) is satisfied, the stress increment is tangent to the yield surface.

Property 2. *A plastic wave traveling with the speed of an elastic wave results in a stress path that is tangent to the yield surface in the stress space. Such a wave is called a neutral wave.*

3. The eigen-value problem in two space dimensions

We now focus on the solid domain $(x_1, x_2, x_3) \in [0, \infty[\times [-h, h] \times [-e, e]$ in a Cartesian coordinate system, where e and h are arbitrary lengths. It is assumed that all quantities depend solely on x_1 and x_2 except the velocity component v_3 that may depend on x_3. In particular, this is the case for $e \ll h$. Furthermore, only plastic simple waves are considered from now on.

The solid is under the plane strain condition $\boldsymbol{\varepsilon} \cdot \boldsymbol{e}_3 = \boldsymbol{0}$ if the velocity $\boldsymbol{v}$ does not depend on x_3 and if v_3 vanishes. Thus, combining the additive partition of the infinitesimal strain tensor: $\boldsymbol{\varepsilon} = \boldsymbol{\varepsilon}^e + \boldsymbol{\varepsilon}^p$, with the elastic law (5) and the kinematic condition $\varepsilon_{33} = 0$, one gets for isotropic materials:

$$\sigma_{33} = \nu (\sigma_{11} + \sigma_{22}) - E \varepsilon_{33}^p \tag{23}$$

Hence, the quasi-linear form (11) reduces for plane strain problems to a system of dimension 5 for the unknowns $v_1, v_2, \sigma_{11}, \sigma_{12}$, and σ_{22}.

The plane stress state $\boldsymbol{\sigma} \cdot \boldsymbol{e}_3 = \boldsymbol{0}$ is assumed if the planes $x_3 = \pm h$ are traction free and $e \ll h$. In that case the stress component σ_{33} is removed from system (11). Nevertheless, the tangent modulus must account for the vanishing out-of-plane stress component by specializing equation (10) to σ_{33}:

$$\dot{\sigma}_{33} = C_{33ij}^{ep} \dot{\varepsilon}_{ij} = 0$$

and therefore:

$$C^{ep}_{3333}\dot{\varepsilon}_{33} = -C^{ep}_{33ij}\dot{\varepsilon}_{ij} \quad i,j = \{1,2\}$$

since $\varepsilon_{13} = \varepsilon_{23} = 0$ also in plane stress. Hence, the constitutive equations are rewritten by means of a two-dimensional tangent modulus $\widetilde{\mathbb{C}}^{ep}$:

$$\dot{\sigma}_{ij} = \left(C^{ep}_{ijkl} - \frac{C^{ep}_{ij33}C^{ep}_{33kl}}{C^{ep}_{3333}}\right)\dot{\varepsilon}_{kl} = \widetilde{C}^{ep}_{ijkl}\dot{\varepsilon}_{kl} \quad i,j,k,l = \{1,2\}$$

The characteristic structure of the problem is then governed by the associated acoustic tensor $\widetilde{\boldsymbol{A}}^{ep} = \boldsymbol{n}\cdot\widetilde{\mathbb{C}}^{ep}\cdot\boldsymbol{n}$.

The removal of σ_{33} from system (11) for both plane strain and plane stress situations allows solving the problem in a two-dimensional setting. Then, generically denoting the acoustic tensor by $\boldsymbol{A}$, the characteristic structures are given by the eigenvalues:

$$\omega_1 = \frac{A_{11} + A_{22} + \sqrt{(A_{11}-A_{22})^2 + 4{A_{12}}^2}}{2} \tag{24}$$

$$\omega_2 = \frac{A_{11} + A_{22} - \sqrt{(A_{11}-A_{22})^2 + 4{A_{12}}^2}}{2} \tag{25}$$

and the associated left eigenvectors:

$$\boldsymbol{l}^1 = [A_{22} - \omega_1\ ,\ -A_{12}]\ ;\ \boldsymbol{l}^2 = [-A_{12}\ ,\ A_{11} - \omega_2] \tag{26}$$

From equation (17), we see that two families of waves with celerities $c_f = \pm\sqrt{\omega_1/\rho}$ and $c_s = \pm\sqrt{\omega_2/\rho}$ may travel in the domain. These waves are respectively referred to as fast and slow waves. One easily shows that property 1 can be particularized to two-dimensional problems and yields: $c_1 \geq c_f \geq c_2 \geq c_s$, where c_1 and c_2 are the speeds of elastic pressure and shear waves respectively.

Remark 1. *Given the non-linearity of $\mathbb{C}^{ep}$ and the mathematical complexity of equations* (24) *and* (25)*, the following assumptions are made in what follows:*

(i) c_f and c_s monotonically decrease with the hardening of the material,

(ii) the computational domain is in an initial natural, plastic strain free state.

Given the eigenvalues (24) and (25), the four left eigenfields of the Jacobian matrix read:

$$\left\{\pm c_f;\quad \mathcal{L}^{c_f^{\pm}} = \left[\ \pm\rho c_f \boldsymbol{l}^1, -\boldsymbol{l}^1\otimes\boldsymbol{n}\ \right]\right\}$$
$$\left\{\pm c_s;\quad \mathcal{L}^{c_s^{\pm}} = \left[\ \pm\rho c_s \boldsymbol{l}^2, -\boldsymbol{l}^2\otimes\boldsymbol{n}\ \right]\right\}$$

where $\mathcal{L}^{c_f^+}$ and $\mathcal{L}^{c_f^-}$ are associated with the right-going and left-going fast waves respectively. The same goes for $\mathcal{L}^{c_s^+}$ and $\mathcal{L}^{c_s^-}$. Furthermore, one stationary wave associated with the zero eigenvalue of the Jacobian matrix, and whose left eigenvector satisfies equation (18), has to be added:

$$\mathcal{L}^{0^T} = \begin{bmatrix} 0 \\ 0 \\ \left(C_{121i}C_{222j} - C_{221i}C_{122j}\right)n_i n_j \\ \left(C_{111i}C_{122j} - C_{112i}C_{121j}\right)n_i n_j \\ \left(C_{112i}C_{221j} - C_{111i}C_{222j}\right)\frac{n_i n_j}{2} \end{bmatrix} = \begin{bmatrix} 0 \\ 0 \\ \alpha_{11} \\ \alpha_{22} \\ \alpha_{12} \end{bmatrix} \tag{27}$$

with $\mathbb{C} = \mathbb{C}^{ep}$ for plane strain and $\mathbb{C} = \widetilde{\mathbb{C}}^{ep}$ for plane stress situations. The above eigenfields are used in the next section in order to derive the simple wave solutions by means of the method of characteristics [35].

4. Integral curves for two-dimensional problems

Solving the hyperbolic system (11) amounts to construct hyper-surfaces $\mathfrak{Q}(x_n, t)$, or integral surfaces, given some initial values $\mathfrak{Q}(x_n, 0)$, which is in general difficult. Nevertheless, the projection of system (11) onto the left eigenbasis leads to the set of characteristic equations [35]:

$$\mathcal{L}^K \cdot d\mathfrak{Q} = 0 \tag{28}$$

where $d\mathfrak{Q}$ is related to the directional derivative of $\mathfrak{Q}$ along the Kth characteristic curve with slope $x_n/t = c_K$ in the (x_n, t) plane. The integration of the set of ODEs (28) yields integral curves that enable, through the method of characteristics, the calculation of self-similar solutions.

In what follows, the construction of the integral curves as well as the application of the method of characteristics are developed for general two-dimensional problems as a first result of the present paper.

The projection of the quasilinear form (11) onto the left eigenbasis developed in the previous section yields for the fast waves:

$$\rho c_f \boldsymbol{l}^1 \cdot d\boldsymbol{v} - l_i^1 n_j d\sigma_{ij} = 0\,, \quad x_n/t = c_f \tag{29}$$

$$-\rho c_f \boldsymbol{l}^1 \cdot d\boldsymbol{v} - l_i^1 n_j d\sigma_{ij} = 0\,, \quad x_n/t = -c_f \tag{30}$$

for the slow waves:

$$\rho c_s \boldsymbol{l}^2 \cdot d\boldsymbol{v} - l_i^2 n_j d\sigma_{ij} = 0\,, \quad x_n/t = c_s \tag{31}$$

$$-\rho c_s \boldsymbol{l}^2 \cdot d\boldsymbol{v} - l_i^2 n_j d\sigma_{ij} = 0\,, \quad x_n/t = -c_s \tag{32}$$

and at last, for the stationary wave:

$$\alpha_{11} d\sigma_{11} + \alpha_{12} d\sigma_{12} + \alpha_{22} d\sigma_{22} = 0\,, \quad x_n/t = 0 \tag{33}$$

Analogously to [8], the method of characteristics is applied by combining equations (29) to (33). The approach

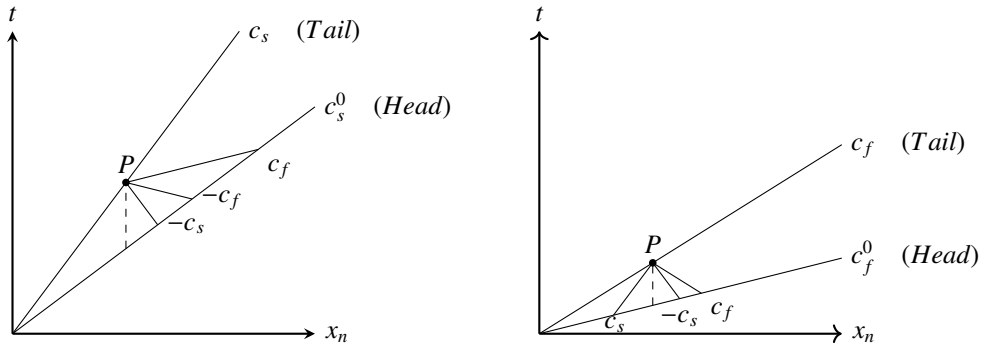

(a) Slow simple wave (b) Fast simple wave

Figure 1: The method of characteristics through slow and fast simple waves in the (x_n, t) plane.

consists in tracing every characteristic from some downstream point of a wave where the state vector $\mathfrak{Q}$ is known, to an upstream point where the solution is sought. Figures 1a and 1b schematically illustrate the method for slow and fast simple waves in which the state is known along the head wave and is looked for at the point P lying on the tail wave.

The right-going slow waves are first looked at by adding equations (29) and (30):

$$l_i^1 n_j d\sigma_{ij} = 0$$

Given the geometry of the problem, the vector $\boldsymbol{n}$ may be reduced to $\boldsymbol{e}_1$ or $\boldsymbol{e}_2$. It therefore comes out:

$$d\sigma_{11} = -\frac{l_2^1}{l_1^1} d\sigma_{12} = \psi_1^s d\sigma_{12} \quad \text{for } \boldsymbol{n} = \boldsymbol{e}_1 \tag{34}$$

$$d\sigma_{22} = -\frac{l_1^1}{l_2^1} d\sigma_{12} = \psi_2^s d\sigma_{12} \quad \text{for } \boldsymbol{n} = \boldsymbol{e}_2 \tag{35}$$

where ψ_1^s and ψ_2^s are functions of all components of $\boldsymbol{\sigma}$. Note that the s and f superscripts stand for slow and fast waves respectively in the following. Next, the characteristic equation related to the contact wave (33) reads:

$$d\sigma_{22} = -\frac{\psi_1^s \alpha_{11} + \alpha_{12}}{\alpha_{22}} d\sigma_{12} \quad \text{for } \boldsymbol{n} = \boldsymbol{e}_1 \tag{36}$$

$$d\sigma_{11} = -\frac{\psi_2^s \alpha_{22} + \alpha_{12}}{\alpha_{11}} d\sigma_{12} \quad \text{for } \boldsymbol{n} = \boldsymbol{e}_2 \tag{37}$$

in which the α_{ij}'s are defined in (27). The sets of equations (34)-(36) and (35)-(37) show the combined-stress nature of slow simple waves since both longitudinal and transverse components vary, in contrast with elastic waves. On the other hand, the subtraction of equations (29) and (30) leads to:

$$dv_1 = \psi_1^s dv_2 = \frac{1}{\psi_2^s} dv_2$$

which, once combined with equations (34)-(35) and introduced in (32), yields after simplifications:

$$dv_1 = -\frac{d\sigma_{11}}{\rho c_s^2} \quad ; \quad dv_2 = -\frac{d\sigma_{12}}{\rho c_s^2} \qquad \text{for } \boldsymbol{n} = \boldsymbol{e}_1 \tag{38}$$

$$dv_1 = -\frac{d\sigma_{12}}{\rho c_s^2} \quad ; \quad dv_2 = -\frac{d\sigma_{22}}{\rho c_s^2} \qquad \text{for } \boldsymbol{n} = \boldsymbol{e}_2 \tag{39}$$

Remark 2. *The ODEs through a left-going slow wave result from the combination of equations* (34)-(35) *introduced in* (31) *rather than* (32)*. Therefore, the only difference lies in the signs in equations* (38) *and* (39)*.*

Similar results are obtained for right-going fast simple waves by using $\boldsymbol{l}^2$ instead of $\boldsymbol{l}^1$ and c_f rather than c_s. Hence, the evolution in slow and fast waves is governed by the *loading functions*:

$$\begin{aligned} \psi_1^s &= -\left.\frac{l_2^1}{l_1^1}\right|_{\boldsymbol{n}=\boldsymbol{e}_1} \quad , \quad \psi_2^s = -\left.\frac{l_1^1}{l_2^1}\right|_{\boldsymbol{n}=\boldsymbol{e}_2} \\ \psi_1^f &= -\left.\frac{l_2^2}{l_1^2}\right|_{\boldsymbol{n}=\boldsymbol{e}_1} \quad , \quad \psi_2^f = -\left.\frac{l_1^2}{l_2^2}\right|_{\boldsymbol{n}=\boldsymbol{e}_2} \end{aligned} \tag{40}$$

The ODEs satisfied across right-going slow and fast simple waves depending on the direction considered are summarized in table 1 for directions $\boldsymbol{e}_1$ and $\boldsymbol{e}_2$.

The complete solution is given by the integral curves that result from the integration of those ODEs. For instance, through a right-going wave in the direction $\boldsymbol{e}_1$, the velocity obeys:

$$v_1 = v_1^0 - \int_{\boldsymbol{\sigma}^0}^{\boldsymbol{\sigma}} \frac{d\sigma_{11}}{\rho c^2} \quad ; \quad v_2 = v_2^0 - \int_{\boldsymbol{\sigma}^0}^{\boldsymbol{\sigma}} \frac{d\sigma_{12}}{\rho c^2} \tag{41}$$

where the zero superscript denotes the downstream state. As emphasized by Clifton [8], the integrals depend on the loading path and hence, the simple waves involved. It is therefore crucial to identify the stress path followed to properly compute integrals (41).

Right-going slow wave		Right-going fast wave	
$\boldsymbol{n} = \boldsymbol{e}_1$	$\boldsymbol{n} = \boldsymbol{e}_2$	$\boldsymbol{n} = \boldsymbol{e}_1$	$\boldsymbol{n} = \boldsymbol{e}_2$
$dv_1 = -\frac{d\sigma_{11}}{\rho c_s^2}$	$dv_1 = -\frac{d\sigma_{12}}{\rho c_s^2}$	$dv_1 = -\frac{d\sigma_{11}}{\rho c_f^2}$	$dv_1 = -\frac{d\sigma_{12}}{\rho c_f^2}$
$dv_2 = -\frac{d\sigma_{12}}{\rho c_s^2}$	$dv_2 = -\frac{d\sigma_{22}}{\rho c_s^2}$	$dv_2 = -\frac{d\sigma_{12}}{\rho c_f^2}$	$dv_2 = -\frac{d\sigma_{22}}{\rho c_f^2}$
$d\sigma_{11} = \psi_1^s d\sigma_{12}$	$d\sigma_{11} = -\frac{\psi_2^s \alpha_{22} + \alpha_{12}}{\alpha_{11}} d\sigma_{12}$	$d\sigma_{11} = \psi_1^f d\sigma_{12}$	$d\sigma_{11} = -\frac{\psi_2^f \alpha_{22} + \alpha_{12}}{\alpha_{11}} d\sigma_{12}$
$d\sigma_{22} = -\frac{\psi_1^s \alpha_{11} + \alpha_{12}}{\alpha_{22}} d\sigma_{12}$	$d\sigma_{22} = \psi_2^s d\sigma_{12}$	$d\sigma_{22} = -\frac{\psi_1^f \alpha_{11} + \alpha_{12}}{\alpha_{22}} d\sigma_{12}$	$d\sigma_{22} = \psi_2^f d\sigma_{12}$

Table 1: Summary of the ODEs satisfied inside right-going slow and fast simple waves.

Remark 3. *Considering the elastic stiffness tensor in the above developments, the equations of elasticity, for which $c_s = c_2$ and $c_f = c_1$, can be derived. In that case, one shows that $\psi_1^s = \psi_2^s = 0$ and $\psi_1^f = \psi_2^f = \infty$, so that the equations of table 1 greatly simplify. As a result, jump conditions associated with discontinuous contact waves are written rather than integral curves such as* (41) *linked to rarefaction waves, which is due to the path-independent constitutive equations. It then turns out that a pressure wave carries jump discontinuities of σ_{nn}, σ_{tt} and v_n, where n and t denote normal and transverse components of the propagation direction, whereas a shear wave propagates jump discontinuities in σ_{nt} and v_t (see table 2).*

Right-going shear wave		Right-going pressure wave	
$\boldsymbol{n} = \boldsymbol{e}_1$	$\boldsymbol{n} = \boldsymbol{e}_2$	$\boldsymbol{n} = \boldsymbol{e}_1$	$\boldsymbol{n} = \boldsymbol{e}_2$
$[\![v_1]\!] = 0$	$[\![v_1]\!] = -\frac{[\![\sigma_{12}]\!]}{\rho c_2^2}$	$[\![v_1]\!] = -\frac{[\![\sigma_{11}]\!]}{\rho c_1^2}$	$[\![v_1]\!] = 0$
$[\![v_2]\!] = -\frac{[\![\sigma_{12}]\!]}{\rho c_2^2}$	$[\![v_2]\!] = 0$	$[\![v_2]\!] = 0$	$[\![v_2]\!] = -\frac{[\![\sigma_{22}]\!]}{\rho c_1^2}$
$[\![\sigma_{11}]\!] = 0$	$[\![\sigma_{11}]\!] = 0$	$[\![\sigma_{12}]\!] = 0$	$[\![\sigma_{12}]\!] = 0$
$[\![\sigma_{22}]\!] = 0$	$[\![\sigma_{22}]\!] = 0$	$[\![\sigma_{22}]\!] = -\frac{\alpha_{11}}{\alpha_{22}}[\![\sigma_{11}]\!]$	$[\![\sigma_{11}]\!] = -\frac{\alpha_{22}}{\alpha_{11}}[\![\sigma_{22}]\!]$

Table 2: Summary of the jump conditions across right-going elastic shear and pressure waves.

5. Some properties of the loading paths for several cases

It has been highlighted that the complete solution of a hyperbolic system in elastic-plastic solids requires to know *a priori* the wave structure. The object of this section is to study the mathematical properties of the loading functions (40) in order to get some clues about the stress paths. It is believed that the information thus earned could be used to accurately approximate the integration of equations (41). First, general properties holding regardless of the loading conditions are highlighted. Next, the equations are specialized to plane stress and plane strain cases.

5.1. The general case

To begin with, let us look at the product of the two loading functions in a direction of space. Given the left eigenvectors of the acoustic tensor in equation (26), one has for instance:

$$\psi_1^s \psi_1^f = \frac{l_2^1}{l_1^1} \frac{l_2^2}{l_1^2}$$

Since the eigenvectors of symmetric second-order tensors all satisfy $\boldsymbol{l}^1 \cdot \boldsymbol{l}^2 = 0$, it comes out that the above product is equal to -1. Hence, the loading paths resulting from the integration of the ODEs involving ψ_1^s and ψ_1^f are perpendicular

in the stress space. The same goes for ψ_2^s and ψ_2^f. Although this orthogonality has already been noticed for particular plane strain and plane stress cases [8, 11], *the generic formulation proposed here shows that this is valid for all problems in two space dimensions*. As a result, the study can be restricted to one function in each direction, say ψ_1^s and ψ_2^s.

Second, if the function ψ_1^s vanishes at some point of the stress space, the projection in the $(\sigma_{11}, \sigma_{12})$ plane of the loading path followed within a slow wave is vertical according to the ODE (34) (*i.e* $d\sigma_{11} = 0$). Conversely, if $\psi_1^s \to \infty$, the loading path is horizontal in the $(\sigma_{11}, \sigma_{12})$ plane (*i.e* $d\sigma_{12} = 0$). These situations respectively correspond to:

$$\psi_1^s = 0 \Leftrightarrow A_{12} = 0$$
$$\psi_1^s \to \infty \Leftrightarrow A_{22} - \omega_1 = 0$$

In particular, if $A_{12} = 0$ the denominator of ψ_1^s reads:

$$A_{22} - \omega_1 = \frac{1}{2}\left(A_{22} - A_{11} - \sqrt{(A_{11} - A_{22})^2 + 4A_{12}^2}\right) = \frac{1}{2}\left(A_{22} - A_{11} - |A_{11} - A_{22}|\right) = -\langle A_{11} - A_{22}\rangle$$

where $\langle\bullet\rangle = \frac{1}{2}(\bullet + |\bullet|)$ denotes the positive part operator. Therefore, if $A_{12} = 0$ and $A_{11} \neq A_{22}$, one has $\psi_1^s = 0$ and hence $\psi_1^f \to -\infty$ by orthogonality. If moreover $A_{11} = A_{22}$, both components of the eigenvectors vanish and the functions ψ_1^s and ψ_1^f are undetermined. Note also that in this case, the characteristic speeds of simple waves are identical according to equations (24) and (25). As a result, the situation $c_f = c_s$ corresponds to a loss of hyperbolicity of the system.

Analogously, the function ψ_2^s is such that:

$$\psi_2^s \to \infty \Leftrightarrow A_{12} = 0$$
$$\psi_2^s = 0 \Leftrightarrow A_{22} - \omega_1 = 0$$

Therefore, if both conditions $A_{12} = 0$ and $A_{11} = A_{22}$ are satisfied, the system is no longer hyperbolic with characteristic speeds of fast and slow waves that are identical.

According to the ODEs of table 1, the particular values of the loading functions $\psi_i^{s,f}$ through the simple waves propagating in direction $\boldsymbol{e}_i$ for $i = \{1, 2\}$, provide information about the loading paths in the stress space. First, $\psi_i^{s,f} = 0$ leads to $d\sigma_{ii} = 0$ (no sum on i) so that the longitudinal stress is constant within the simple wave. Conversely, with the loading functions tending to infinity, the stress σ_{12} does not vary. Notice that the coefficients α_{ij} of the left eigenvector of the Jacobian matrix associated with the zero eigenvalue (27) also have to be regarded. Nevertheless, those terms resulting from products of the components of the elastoplastic tangent modulus have complex expressions and are assumed to have non-zero values in the remainder of the paper.

The above discussions are now specified to the plane strain and plane stress cases, for which loading conditions leading to $A_{12} = 0$ and $A_{11} - A_{22} = 0$ are identified.

5.2. The plane strain case

The case of plane strain is first considered by using the elastoplastic tangent modulus so that the components of the acoustic tensor for $\boldsymbol{n} = \boldsymbol{e}_1$ read:

$$A_{11}^{ep} = C_{1111}^{ep} = \lambda + 2\mu - \beta s_{11}^2 \tag{42}$$
$$A_{22}^{ep} = C_{2121}^{ep} = \mu - \beta s_{12}^2 \tag{43}$$
$$A_{12}^{ep} = C_{1121}^{ep} = -\beta s_{11} s_{12} \tag{44}$$

The associated eigenvalues are then:

$$\rho c_s^2 = -\frac{\sqrt{\left[\lambda + \mu - \beta(s_{11}^2 - s_{12}^2)\right]^2 + 4(\beta s_{11} s_{12})^2}}{2} + \frac{\lambda + 3\mu - \beta(s_{11}^2 + s_{12}^2)}{2} \tag{45}$$

$$\rho c_f^2 = \frac{\sqrt{\left[\lambda + \mu - \beta(s_{11}^2 - s_{12}^2)\right]^2 + 4(\beta s_{11} s_{12})^2}}{2} + \frac{\lambda + 3\mu - \beta(s_{11}^2 + s_{12}^2)}{2} \tag{46}$$

Subtracting equations (42) and (43), one gets: $A^{ep}_{11} - A^{ep}_{22} = \lambda + \mu - \beta\left(s^2_{11} - s^2_{12}\right)$. Hence, the equation $A^{ep}_{11} - A^{ep}_{22} = 0$ admits a set of solutions in the deviatoric stress space. On the other hand, we see from equation (44) that A^{ep}_{12} vanishes for $s_{12} = 0$ or $s_{11} = 0$. Each solution is studied in more details below.

5.2.1. Condition $s_{12} = 0$

According to equations (45) and (46), the eigenvalues of the acoustic tensor become:

$$\rho c_s^2 = \frac{1}{2}\left(\lambda + 3\mu - \beta s^2_{11} - \left|\lambda + \mu - \beta s^2_{11}\right|\right)$$
$$\rho c_f^2 = \frac{1}{2}\left(\lambda + 3\mu - \beta s^2_{11} + \left|\lambda + \mu - \beta s^2_{11}\right|\right)$$

Two cases are to be considered:

(i) if $\beta s^2_{11} < \lambda + \mu$, the expression further reduces to:

$$\rho c_s^2 = \mu$$
$$\rho c_f^2 = \lambda + 2\mu - \beta s^2_{11}$$

The characteristic speed of slow waves is therefore equivalent to that of elastic shear waves for plane strain $c_s = c_2 = \sqrt{\mu/\rho}$.

(ii) if $\lambda + \mu - \beta s^2_{11} < 0$, the characteristic speeds read:

$$\rho c_s^2 = \lambda + 2\mu - \beta s^2_{11}$$
$$\rho c_f^2 = \mu$$

Therefore, the celerity of fast waves reduces to that of elastic shear waves. Note, however, that the characteristic speed of slow waves remains real if and only if $\lambda + 2\mu > \beta s^2_{11}$. One then gets the following bounds: $\lambda + 2\mu > \beta s^2_{11} > \lambda + \mu$.

Note that the two above situations lead to the propagation of one neutral wave in the medium.

At last, the equality $\beta s^2_{11} = \lambda + \mu$ leads to $A^{ep}_{11} - A^{ep}_{22} = 0$ and hence, to undetermined loading functions.

5.2.2. Condition $s_{11} = 0$

Considering the relation (23) between the stress components for plane strain, one writes:

$$s_{11} = \frac{2}{3}\sigma_{11} - \frac{1}{3}(\sigma_{22} + \nu(\sigma_{11} + \sigma_{22}) - E\varepsilon^p_{33})$$

so that $s_{11} = 0$ is equivalent to:

$$\sigma_{11} = \frac{1+\nu}{2-\nu}\sigma_{22} - E\varepsilon^p_{33} \tag{47}$$

In contrast to what has been seen previously, the functions $\psi^{s,f}$ cannot be undetermined in the case $s_{11} = 0$ since the equation $A^{ep}_{11} - A^{ep}_{22} = \lambda + \mu + \beta s^2_{12} = 0$ does not admit real solutions. Nevertheless, the stress state (47) yields the following characteristic speeds:

$$\rho c_s^2 = \mu - \beta s^2_{12}$$
$$\rho c_f^2 = \lambda + 2\mu$$

so that the celerity of fast waves identifies with that of elastic pressure waves under plane strain $c_f = c_1 = \sqrt{(\lambda + 2\mu)/\rho}$. Once again, this case corresponds to the propagation of a neutral wave.

The same analysis can be carried out in the direction $\boldsymbol{n} = \boldsymbol{e}_2$ by considering the following acoustic tensor components:

$$\begin{aligned} A^{ep}_{11} &= C^{ep}_{1212} = \mu - \beta s^2_{12} \\ A^{ep}_{22} &= C^{ep}_{2222} = \lambda + 2\mu - \beta s^2_{22} \\ A^{ep}_{12} &= C^{ep}_{1222} = -\beta s_{22} s_{12} \end{aligned}$$

The characteristic speeds are then:

$$\begin{aligned} \rho c_s^2 &= -\frac{\sqrt{\left[\lambda + \mu - \beta(s^2_{22} - s^2_{12})\right]^2 + 4(\beta s_{22} s_{12})^2}}{2} + \frac{\lambda + 3\mu - \beta(s^2_{22} + s^2_{12})}{2} \\ \rho c_f^2 &= \frac{\sqrt{\left[\lambda + \mu - \beta(s^2_{22} - s^2_{12})\right]^2 + 4(\beta s_{22} s_{12})^2}}{2} + \frac{\lambda + 3\mu - \beta(s^2_{22} + s^2_{12})}{2} \end{aligned}$$

With these expressions, the same remarks as for $\boldsymbol{n} = \boldsymbol{e}_1$ can obviously be made by replacing s_{11} with s_{22}.

Among the above results, the most significant arises from the condition $s_{12} = 0$. Indeed, it has been seen that $A^{ep}_{12} = 0$ leads to $\psi^s_1 = 0$ and $\psi^s_2 \to \infty$ in such a way that the corresponding loading paths in the $(\sigma_{11}, \sigma_{12})$ plane are respectively vertical and horizontal. Under the orthogonality property of the loading functions, the stress path followed in a fast wave propagating in the direction $\boldsymbol{e}_1$ is horizontal in the same plane. Hence, if the path through a fast wave intersects the plane $\sigma_{12} = 0$, the shear stress component remains constant afterwards. The same result holds for the slow wave propagating in the direction $\boldsymbol{e}_2$. The above conclusion are summarized in table 3.

	Stress path in $(\sigma_{11}, \sigma_{12})$ plane for $\sigma_{12} = 0$	
	$\boldsymbol{n} = \boldsymbol{e}_1$ $(i = 1)$	$\boldsymbol{n} = \boldsymbol{e}_2$ $(i = 2)$
Slow wave: $\frac{d\sigma_{ii}}{d\sigma_{12}} = \psi^s_i$ ($i = \{1, 2\}$ no sum on i)	$\psi^s_1 = 0 \Rightarrow$ vertical path	$\psi^s_2 \to \infty \Rightarrow$ horizontal path
Fast wave: $\frac{d\sigma_{ii}}{d\sigma_{12}} = \psi^f_i$ ($i = \{1, 2\}$ no sum on i)	$\psi^f_1 \to \infty \Rightarrow$ horizontal path	$\psi^f_2 = 0 \Rightarrow$ vertical path

Table 3: Loading paths projected on the $(\sigma_{11}, \sigma_{12})$ plane followed across slow and fast simple waves, under the condition $\sigma_{12} = 0$ assuming that $A^{ep}_{11} - A^{ep}_{22} \neq 0$.

5.3. The plane stress case

As mentioned in section 3, a suitable elastoplastic tangent modulus $\widetilde{\mathbb{C}}^{ep}$ is now under consideration. Let's first focus on ψ^s_1 related to the vector $\boldsymbol{n} = \boldsymbol{e}_1$. Thus:

$$\widetilde{A}^{ep}_{11} = C^{ep}_{1111} - \frac{(C^{ep}_{1133})^2}{C^{ep}_{3333}} = \lambda + 2\mu - \beta s^2_{11} - \frac{(\lambda - \beta s_{11} s_{33})^2}{\lambda + 2\mu - \beta s^2_{33}} \tag{48}$$

$$\widetilde{A}^{ep}_{22} = C^{ep}_{2121} - \frac{(C^{ep}_{2133})^2}{C^{ep}_{3333}} = \mu - \beta s^2_{12} - \frac{(\beta s_{12} s_{33})^2}{\lambda + 2\mu - \beta s^2_{33}} \tag{49}$$

$$\widetilde{A}^{ep}_{12} = C^{ep}_{1121} - \frac{C^{ep}_{1133} C^{ep}_{1233}}{C^{ep}_{3333}} = \beta s_{12} \frac{\lambda s_{33} - (\lambda + 2\mu) s_{11}}{\lambda + 2\mu - \beta s^2_{33}} \tag{50}$$

In order to ensure the hyperbolicity of the system, the components of the acoustic tensor also have to be defined, that is $C^{ep}_{3333} > 0$, which leads to:

$$\lambda + 2\mu - \beta s^2_{33} > 0 \quad \Leftrightarrow \quad s^2_{33} < \frac{\lambda + 2\mu}{\beta}$$

Second, from equation (50), $\widetilde{A}^{ep}_{12}$ admits two roots in terms of the components of the deviatoric stress tensor, namely:

$$s_{12} = 0 \quad ; \quad s_{11} = \frac{\lambda}{\lambda + 2\mu} s_{33}$$

In terms of the components of the Cauchy stress tensor, these conditions read:

$$\sigma_{12} = 0 \quad ; \quad \sigma_{11} = \frac{2\mu}{3\lambda + 4\mu} \sigma_{22}$$

If on the other hand the vector $\boldsymbol{n} = \boldsymbol{e}_2$ is considered, the acoustic tensor components read:

$$\widetilde{A}^{ep}_{11} = C^{ep}_{1212} - \frac{(C^{ep}_{1233})^2}{C^{ep}_{3333}} = \mu - \beta s_{12}^2 - \frac{(\lambda - \beta s_{12} s_{33})^2}{\lambda + 2\mu - \beta s_{33}^2}$$
$$\widetilde{A}^{ep}_{22} = C^{ep}_{2222} - \frac{(C^{ep}_{2233})^2}{C^{ep}_{3333}} = \lambda + 2\mu - \beta s_{22}^2 - \frac{(\beta s_{22} s_{33})^2}{\lambda + 2\mu - \beta s_{33}^2}$$
$$\widetilde{A}^{ep}_{12} = C^{ep}_{1222} - \frac{C^{ep}_{1233} C^{ep}_{2233}}{C^{ep}_{3333}} = \beta s_{12} \frac{\lambda s_{33} - (\lambda + 2\mu) s_{22}}{\lambda + 2\mu - \beta s_{33}^2}$$

These expressions are similar to those obtained before with s_{22} instead of s_{11}. It comes out that $\widetilde{A}^{ep}_{12}$ admits two roots in the case $\boldsymbol{n} = \boldsymbol{e}_2$:

$$\sigma_{12} = 0 \quad ; \quad \sigma_{22} = \frac{2\mu}{3\lambda + 4\mu} \sigma_{11}$$

The complexity introduced by the plane stress tangent modulus prevents finding other singular configurations for the hyperbolic system. In particular, it is difficult to deal with the equation $\widetilde{A}^{ep}_{11} = \widetilde{A}^{ep}_{22}$ due to the expressions given in equations (48) and (49). Nevertheless, since the stress state $s_{12} = 0$ also constitutes a singular point for plane stress, the same remarks as those made for the plane strain loading path hold. Namely, σ_{12} becomes constant if it falls to zero along the loading path followed inside a fast (*resp. slow*) wave propagating in direction $\boldsymbol{e}_1$ (*resp.* $\boldsymbol{e}_2$), as summarized in table 3.

6. Numerical integration of stress paths

Although some properties of the simple waves have been emphasized in section 5, the complexity of the equations prevents the complete characterization of the loading paths followed. In order to get additional information about the evolution of the stress states, the systems of ODEs gathered in table 1 are here numerically integrated for plane stress and plane strain loadings. Only linear isotropic hardening is considered by setting $R(p) = Cp$ so that $R' = C$, with C the hardening modulus. Then, the thin-walled tube problem considered by Clifton [8] is first looked at so that the above developments can be validated. Next, the plane stress and plane strain cases are treated. The values of the elastic and plastic properties considered are summarized in table 4.

$E = 2 \times 10^{11}\ Pa$	$\sigma^y = 1 \times 10^8 Pa$
$\nu = 0.3$	$C = 10^8 Pa$
$\rho_0 = 7800\ kg.m^{-3}$	

Table 4: Values of the elastic and plastic parameters.

For the following analysis, it is convenient to introduce two quantities that account for the evolution of the speeds of plastic waves:

$$\xi_f = \frac{c_f - c_2}{c_1 - c_2} \quad ; \quad \xi_s = \frac{c_s}{c_2}$$

Given the intervals $c_1 \geq c_f \geq c_2$ and $c_2 \geq c_s > 0$, it is seen that $\xi_f \in [0, 1]$ and $\xi_s \in \,]\,0, 1]$.

6.1. The thin-walled tube problem

Consider the semi-infinite domain in the Cartesian coordinate system: $(x_1, x_2, x_3) \in [0, \infty[\times[-h, h]\times[-e, e]$, being acted upon by a traction vector $\boldsymbol{T}^d$ at $x_1 = 0$ and free surfaces $x_2 = \pm h$ and $x_3 = \pm e$. Only the first two components of $\boldsymbol{T}^d$ are non-null so that the stress and strain tensors within the medium are of the form:

$$\boldsymbol{\sigma} = \begin{bmatrix} \sigma_{11} & \sigma_{12} & 0 \\ & 0 & 0 \\ sym & & 0 \end{bmatrix} \quad ; \quad \boldsymbol{\varepsilon} = \begin{bmatrix} \varepsilon_{11} & \varepsilon_{12} & 0 \\ & \varepsilon_{22} & 0 \\ sym & & \varepsilon_{33} \end{bmatrix}$$

By using the following mapping of coordinates: $(1, 2, 3) \mapsto (z, \theta, r)$, such a state also corresponds to that holding in a hollow cylinder with radius and length much bigger than its thickness, submitted to combined longitudinal and torsional loads. As a particular plane stress case, the set of ODEs along characteristics derived in section 5 applies by taking into account the vanishing stress component σ_{22}:

$$\begin{aligned} & \dot{\sigma}_{22} = \widetilde{C}^{ep}_{22ij}\dot{\varepsilon}_{ij} = 0 \quad i, j = \{1, 2\} \\ \Rightarrow \quad & \widetilde{C}^{ep}_{2222}\dot{\varepsilon}_{22} = -\widetilde{C}^{ep}_{22ij}\dot{\varepsilon}_{ij} \quad ij = \{11, 12, 21\} \end{aligned}$$

where $\widetilde{\mathbb{C}}^{ep}$ is the plane stress tangent modulus already used and based on the property $\varepsilon_{13} = \varepsilon_{23} = 0$. Thus, inverting the above equation and introducing it in the constitutive equation, we are left with the following law:

$$\begin{aligned} & \dot{\sigma}_{ij} = \widetilde{C}^{ep}_{ijkl}\dot{\varepsilon}_{kl} - \frac{\widetilde{C}^{ep}_{ij22}\widetilde{C}^{ep}_{22kl}}{\widetilde{C}^{ep}_{2222}}\dot{\varepsilon}_{kl} = \widehat{C}^{ep}_{ijkl}\dot{\varepsilon}_{kl} \\ & \text{for } \; ij, kl = \{11, 12, 21\} \end{aligned} \tag{51}$$

The characteristic analysis of the hyperbolic system based on this tangent modulus also leads to loading paths followed across slow and fast waves, involving however two components of stress rather than three. For the sake of simplicity, the stress components are denoted by $\sigma_{11} = \sigma$ and $\sigma_{12} = \tau$.

Thus, the ODEs governing the evolution of stress components inside the waves of combined-stress read:

$$d\sigma = \psi^{s,f} d\tau \tag{52}$$

where the loading functions $\psi^{s,f}$ depend on the components of the acoustic tensor that corresponds to the tangent modulus (51). Equations (52) as well as those of Clifton [8] have been numerically integrated, starting from several arbitrary points lying on the initial yield surface. Since the loading functions are odd functions of σ and τ [8], $\tau(\sigma)$ and $\sigma(\tau)$ are even functions and hence, the loading paths exhibit symmetries with respect to τ and σ axes. Therefore, the study is restricted to the quarter-plane ($\sigma > 0, \tau > 0$).

Figure 2 shows one stress path resulting from the integration of the ODE related to right-going fast waves with σ used as a driving parameter. The initial stress state lies on the yield surface at $\sigma = 0$ and the ODE is discretized by means of the backward Euler method, the integration being performed until the stress reaches the value $\sigma = \sigma^y$. The path is depicted in the stress space and in the deviatoric plane in figures 2a and 2b respectively. The deviatoric plane projection is obtained by drawing the paths in the eigenstress space $(\sigma_1, \sigma_2, \sigma_3)$ and projecting them onto the plane perpendicular to the hydrostatic axis $\sigma_1 = \sigma_2 = \sigma_3$. In this plane, the von-Mises yield surface is a circle drawn with dashed lines. As observed by Clifton, the path inside fast waves first follows the initial yield surface up to the intersection with the σ-axis. Then, the loading path is such that $d\tau = 0$ while σ increases as far as hyperbolicity holds, that is for $c_f > c_2 = \sqrt{\mu/\rho}$ [8]. Notice that these conclusions are similar to those made in the previous section. The ODEs derived in section 5 for plane stress, once adapted to the thin walled-tube problem, then yield the solution originally proposed by Clifton.

Adopting the same approach with τ as driving parameter, some stress paths through slow waves have been reported in figure 3. Since fast waves lead to loading paths following the initial yield surface, the orthogonality property of the loading functions implies that those of slow waves move away from it perpendicularly. This is seen in figure 3a. However, this property holds in the (σ, τ) plane but not in the deviatoric plane, as can be seen in figure 3b, since the quasi-linear form (11) and in turn, the ODEs, are not written in terms of s_1, s_2, s_3. As a result, although the loading paths in the deviatoric plane move away from the initial yield surface, those curves are not radial. Generally speaking, these results also show that the equations derived in the present paper are in excellent agreement with the works of Clifton.

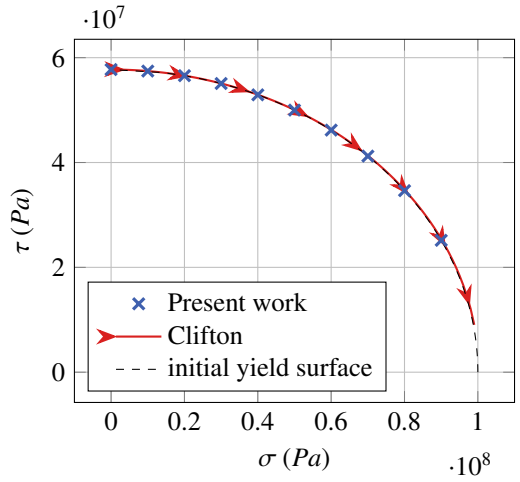

(a) Stress path in (σ, τ) plane

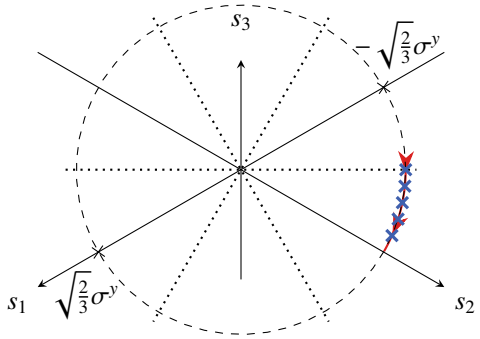

(b) Stress path in deviatoric plane

Figure 2: Stress path followed in a fast simple wave for the thin-walled tube problem. Comparison between the results obtained from equations (52) and these of [8].

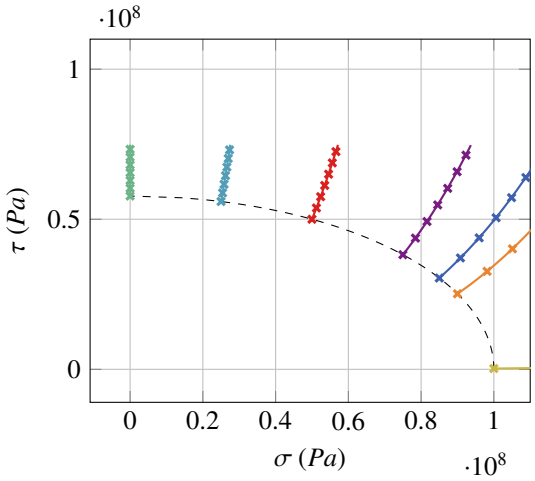

(a) Stress path in (σ, τ) plane

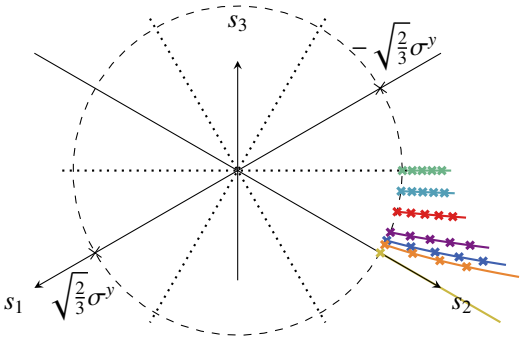

(b) Stress path in deviatoric plane

Figure 3: Loading paths in a slow wave for the thin-walled tube problem. Comparison between the results obtained from equations (52) (cross markers) and those of [8] (solid lines).

6.2. Plane stress

We now move on to a more general plane stress case for which the stress component σ_{22} is not zero. Although the equations of section 5 have been derived for two directions of propagation, attention is paid here to $\boldsymbol{n} = \boldsymbol{e}_1$ only. Thus, the system of ODEs considered reads (see table 1):

$$\begin{aligned} d\sigma_{11} &= \psi_1^{s,f} d\sigma_{12} \\ d\sigma_{22} &= -\frac{\psi_1^{s,f}\alpha_{11} + \alpha_{12}}{\alpha_{22}} d\sigma_{12} \end{aligned} \tag{53}$$

Since the plastic simple waves arise once the plastic threshold has been reached, elastic pressure and shear discontinuities must be considered to bring the stress state on the initial yield surface. As written in table 2, elastic shear waves

have an influence on the shear component σ_{12} only while elastic pressure waves carry jump discontinuities $[\![\sigma_{11}]\!]$ and $[\![\sigma_{22}]\!]$ satisfying:

$$[\![\sigma_{22}]\!] = \frac{\lambda}{2(\lambda+\mu)}[\![\sigma_{11}]\!] \tag{54}$$

Furthermore, the yield function (6) can be written for plane stress as:

$$\sqrt{3\sigma_{12}^2 + (\sigma_{11}^2 + \sigma_{22}^2 - \sigma_{11}\sigma_{22})} - (\sigma^y + C\ p) = 0$$

Then, inverting the above equation allows expressing σ_{12} as a function of the other components on the boundary of the elastic convex:

$$\sigma_{12} = \pm\sqrt{\frac{1}{3}}\sqrt{(\sigma^y + C\ p)^2 - \left(\sigma_{11}^2 + \sigma_{22}^2 - \sigma_{11}\sigma_{22}\right)} \tag{55}$$

Thus, combining the conditions (54) and (55), one can define stress states lying on the initial yield surface by only setting σ_{11}. The initial values set for σ_{11}, and hence these of σ_{22}, form in what follows a symmetrical set with respect to zero. From such states, the ODEs (53) are implicitly integrated with σ_{12} used as a driving parameter and by restricting ourselves to the semi-space $\sigma_{12} > 0$ for the initial conditions.

6.2.1. Fast waves

Following the above approach, the equations holding inside fast waves are first integrated until σ_{12} vanishes. The resulting loading paths are depicted in figure 4 in the $(\sigma_{11}, \sigma_{12})$ and $(\sigma_{22}, \sigma_{12})$ planes, and in the deviatoric plane in figure 5. Note that the curves are numbered so as to facilitate the mapping between the three different planes and the initial yield surface is depicted in dashed line in figure 5. The evolution of the characteristic speed associated with

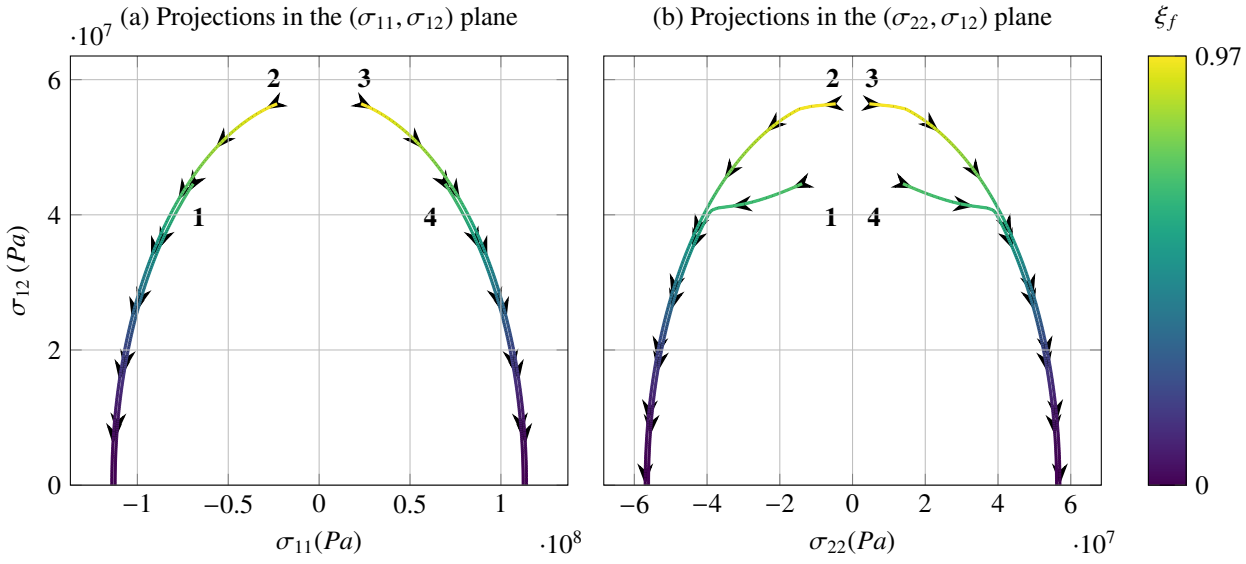

Figure 4: Loading paths in a fast simple wave under plane stress conditions in the stress planes $(\sigma_{11}, \sigma_{12})$ and $(\sigma_{22}, \sigma_{12})$.

the fast wave along the path can also be seen in the figures by means of a color gradient on the variable ξ_f. Thus, for the loadings under consideration, the wave celerity is a decreasing function of the stress so that the simple wave solutions are valid.

First, the negative and positive initial values allow highlighting that σ_{12} is an even function of σ_{11} and σ_{22}, though it is not shown mathematically. Indeed, a symmetry with respect to the σ_{12}-axis can be observed in both $(\sigma_{11}, \sigma_{12})$

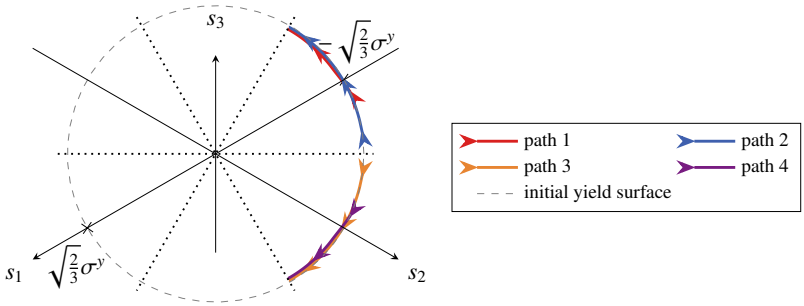

Figure 5: Loading path in a fast simple wave under plane stress conditions in the deviatoric plane.

and $(\sigma_{22}, \sigma_{12})$ planes. On the other hand, the symmetry property is also seen in the deviatoric plane in figure 5 in which positive (*resp. negative*) initial values yield clockwise (*resp. counterclockwise*) loading paths. In addition, as for the thin-walled tube problem, the stress curves follow the initial yield surface up to a direction of pure shear in the deviatoric plane. At that point, the speed of elastic shear waves c_2 is achieved since $\xi_f = 0$. Therefore, it seems that all the loading paths followed in a fast wave aim at reaching a direction of pure shear in the deviatoric plane and cannot be extended further.

6.2.2. Slow waves

We now focus on the stress evolution inside slow waves. The same procedure is followed for several starting points on the initial yield surface by increasing σ_{12}. The loading paths thus obtained are depicted in figures 6 and 7, for which projections in the stress space and the deviatoric plane are shown respectively. The evolution of ξ_s along the

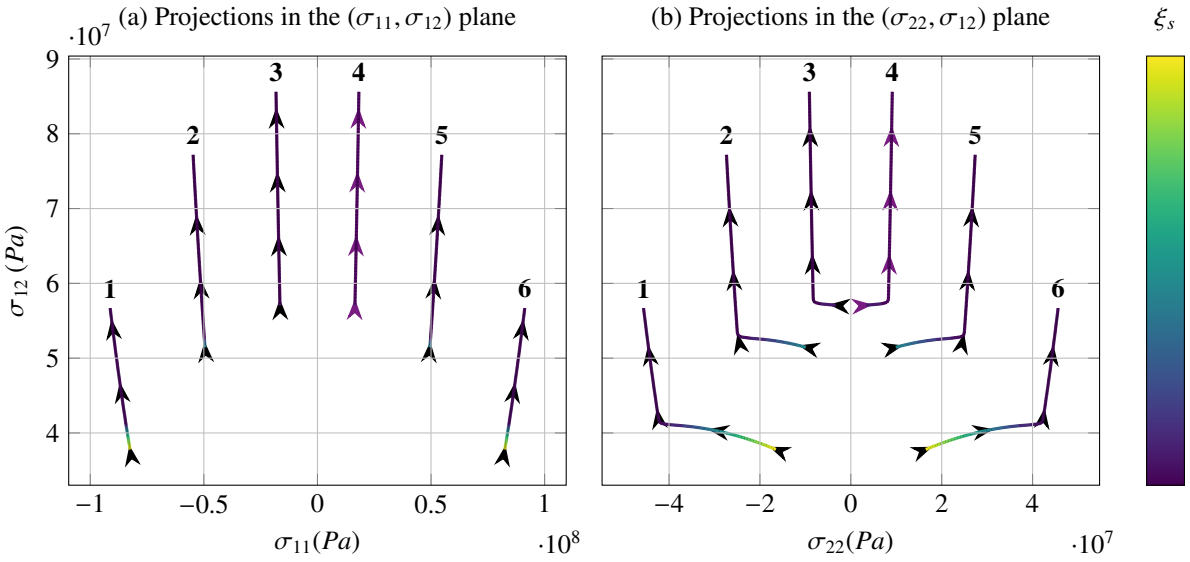

Figure 6: Loading paths in a slow simple wave under plane stress conditions in the stress planes $(\sigma_{11}, \sigma_{12})$ and $(\sigma_{22}, \sigma_{12})$ for several starting points lying on the initial yield surface.

paths in the stress space can also be seen by means of a color gradient. Once again, the simple wave solution appears to be valid with the considered loading conditions. Moreover, no neutral waves are considered since $\xi_s < 1$.

First, generally speaking, the same symmetry properties of the loading paths as for the fast waves can be seen in

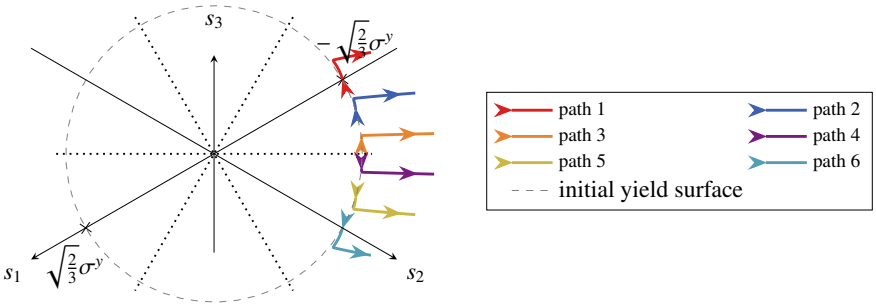

Figure 7: Loading paths in a slow simple wave under plane stress conditions in the deviatoric plane for several starting points lying on the initial yield surface.

the figures. Second, while the projections of the curves in the $(\sigma_{11}, \sigma_{12})$ plane can be pretty well approximated with straight lines, it is not the case in the $(\sigma_{22}, \sigma_{12})$ plane. Indeed, in the latter case, the variations first mainly concern σ_{22} and next, the slopes of the curves roughly change so that the paths are almost vertical. On the other hand, the projections in the deviatoric plane in figure 7 show that the paths start turning around the initial yield surface up to some points where the direction changes. Once the flow direction has changed, the stress state continues moving away from the initial yield surface without following a radial direction. These solutions are much more complex than those of the thin-walled cylinder problem.

Although the slope breaks are not identified by looking at the mathematical properties of the loading function ψ_1^s, one can show numerically that the inflections occur for each path once the condition $\sigma_{11} = 2\sigma_{22}$ is achieved. As a matter of fact, this condition results from the vanishing partial derivative of equation (55) with respect to σ_{22}:

$$\frac{\partial \sigma_{12}}{\partial \sigma_{22}} = \pm \frac{2\sigma_{22} - \sigma_{11}}{6\sigma_{12}} = 0 \tag{56}$$

Considering one slice $\sigma_{11} = constant$ in the stress space, the condition (56) corresponds to the extremum values taken by σ_{12} along the current yield surface. For the von-Mises function, such slices in the $(\sigma_{22}, \sigma_{12})$ plane are ellipses whose vertices satisfy the condition (56). Figure 8 shows the initial yield surface in the stress space as well as the set of points satisfying the condition (56), which is referred to as the *maximum-shear-stress* line. The loading paths studied above are also reported in the figure in such a way that it can be seen that all the integral curves aim at reaching the *maximum-shear-stress* line. It is worth noticing that the paths are not restricted to the initial yield surface in the case of slow waves so that the corresponding curves do not intersect the black line in figure 8. However, since the isotropic hardening has only homothetic effects on the yield surface, the *maximum-shear-stress* line moves in the direction of increasing σ_{12} with the plastic flow, and then seems to intersect the loading paths. In order to confirm these observations, the above discussion is supplemented with other results depicted in figure 9.

First, the ratio $\frac{2\sigma_{22}}{\sigma_{11}}$ is plotted versus the Cauchy stress component σ_{22} along the loading paths in figure 9a. The same response as that shown in figure 6b is observed, namely, a first phase during which σ_{22} varies significantly followed by a second one characterized by a lower variation. This is in particular obvious by looking at the paths 1 and 6. The transition between the two phases occurs at $\frac{2\sigma_{22}}{\sigma_{11}} = 1$. Next, the mapping with the deviatoric plane can be made by looking at the Lode parameter defined as [36]:

$$\cos(3\Theta) = 9\sqrt{\frac{2}{3}}\frac{\det \boldsymbol{s}}{\|\boldsymbol{s}\|^3}$$

The Lode parameter is related to the angular position in the deviatoric plane so that its variation along the loading paths gives information about the plastic flow direction. Figure 9b shows the evolution of the ratio $\frac{2\sigma_{22}}{\sigma_{11}}$ with respect to the Lode parameter. It can be seen that the Lode parameter varies monotonically until condition (56) is fulfilled. After that point, the Lode parameter roughly changes, which explains the breaks in the slope of the curves in figure

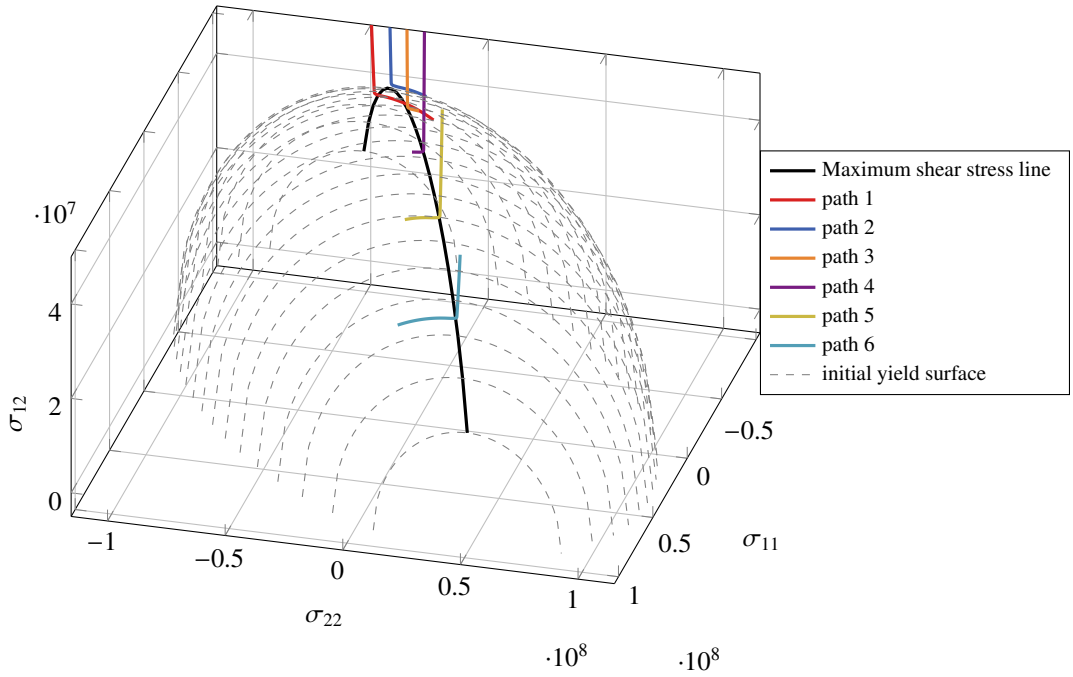

Figure 8: Loading paths through slow waves under plane stress conditions along with the *maximum-shear-stress* line in the stress space.

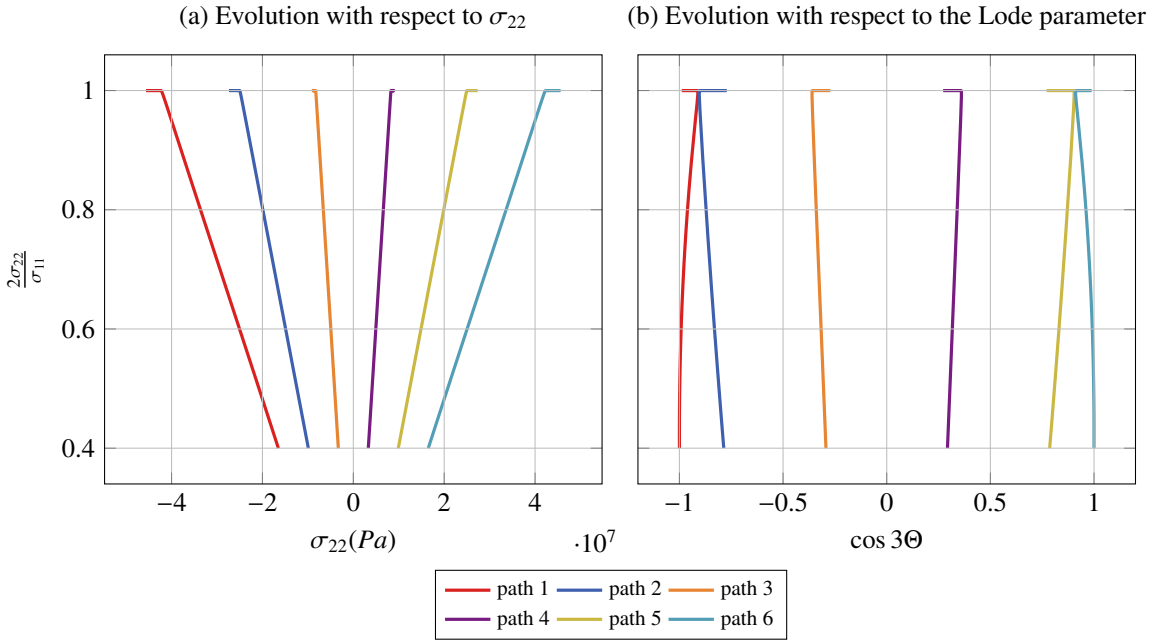

Figure 9: Evolution of the ratio $\frac{2\sigma_{22}}{\sigma_{11}}$ along slow wave loading paths.

7. Note that the inflections that can be seen at the beginning of paths 1 and 6 are due to the evenness of the cosine function. The curves depicted in figure 9 moreover highlight that once the direction of the paths roughly changes, the *maximum-shear-stress* condition remains valid, in such a way that a slow wave aims at following a *maximum-shear-*

stress evolution.

The response emphasized before nevertheless differs for a higher hardening modulus. Therefore, the hardening parameter is momentarily set to $C = 10^{10}$Pa and the same procedure as before is carried out. Figure 10 shows the loading paths resulting from the same initial setup in the deviatoric plane, and the evolution of the ratio $\frac{2\sigma_{22}}{\sigma_{11}}$ is depicted in figure 11. It turns out that increasing the hardening modulus smooth the loading paths so that figure 10 does not exhibit the slope breaks that were seen in figure 7. On the other hand, figure 11 shows that as for the previous case, the

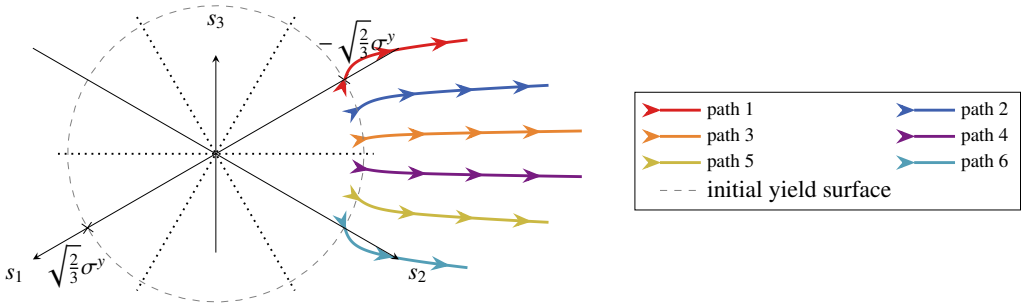

Figure 10: Loading paths in a slow simple wave under plane stress conditions in the deviatoric plane for several starting points lying on the initial yield surface with an increased hardening modulus.

Lode parameter does not vary monotonically along the loading paths. It is however worth noticing that the evolution of the Lode parameter reverses before the *maximum-shear-stress* condition is achieved. It furthermore appears that the paths only tend to the aforementioned condition rather than reaching it.

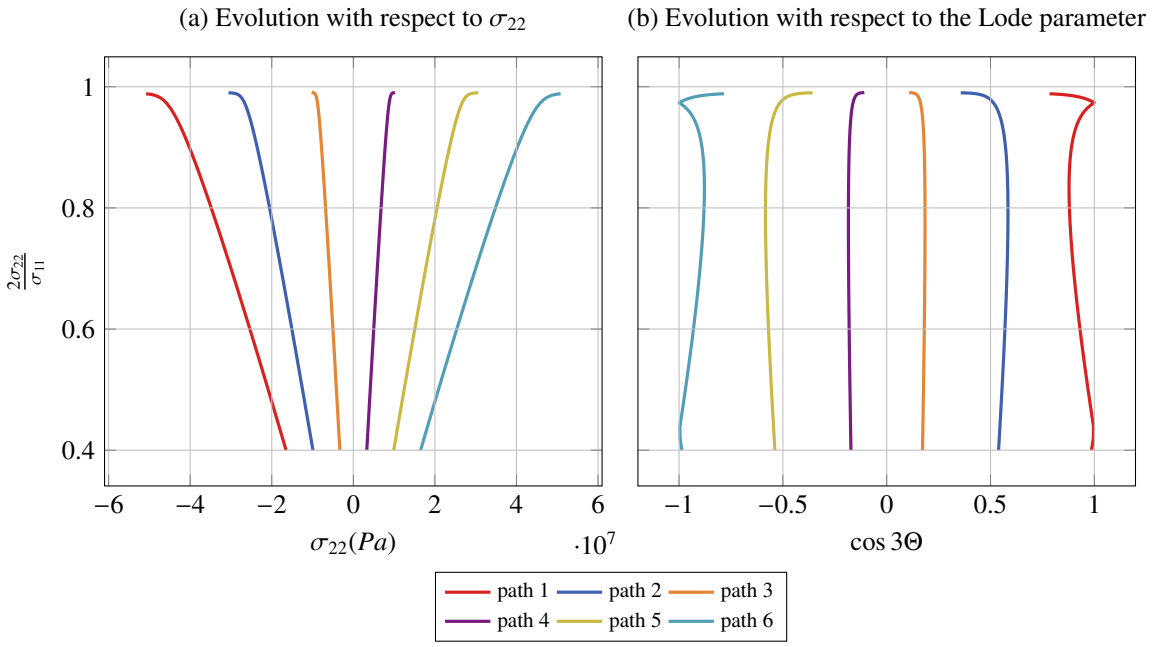

Figure 11: Evolution of the ratio $\frac{2\sigma_{22}}{\sigma_{11}}$ along slow wave loading paths with an increased hardening modulus.

Even though the loading paths are influenced by the value of the hardening modulus, the above results show that the plane stress condition leads to solutions that are very different from those of the thin-walled tube problem for slow waves. However, valuable information have been provided by the numerical results presented above.

6.3. Plane strain

Assuming that a solid initially at rest undergoes external loads leading to a plane strain case, the previous approach is now repeated. However, the derivation of the hyperbolic system in a two-dimensional setting relies on the writing of the out-of-plane stress component as a function of plastic strain. Hence, the integral curves associated with simple waves are integrated implicitly, along with the plastic flow. To do so, the consistency condition of the von-Mises yield surface (6) is combined with the plastic flow rule (9):

$$\dot{\boldsymbol{\varepsilon}}^p = \frac{3}{2C}\frac{\boldsymbol{s}\otimes\boldsymbol{s}}{\|\boldsymbol{s}\|^2} : \dot{\boldsymbol{\sigma}}$$

Thus, the system of ODEs consists of the equations of table 1:

$$d\sigma_{11} = \psi_1^{s,f} d\sigma_{12}$$
$$d\sigma_{22} = -\frac{\psi_1^{s,f}\alpha_{11} + \alpha_{12}}{\alpha_{22}} d\sigma_{12}$$

supplemented with the ODE related to the out-of-plane component which follows from the time derivative of equation (23):

$$d\sigma_{33} = \nu\,(d\sigma_{11} + d\sigma_{22}) - E d\varepsilon_{33}^p$$

Once again, we consider that elastic pressure and shear waves precede plastic ones. Therefore, according to the equations summarized in table 2, the components σ_{11} and σ_{22} are coupled through the pressure wave under plane strain such that:

$$[\![\sigma_{22}]\!] = \frac{\lambda}{\lambda + 2\mu}[\![\sigma_{11}]\!]$$

In addition, one shows that specializing the yield surface to plane strain, by accounting for the expression of the out-of-plane stress (23), leads to:

$$\sqrt{3\sigma_{12}^2 + (\sigma_{11}^2 + \sigma_{22}^2)(\nu^2 - \nu + 1) + \sigma_{11}\sigma_{22}(2\nu^2 - 2\nu - 1) + E\varepsilon_{33}^p\left[(\sigma_{11} + \sigma_{22})(1 - 2\nu) + E\varepsilon_{33}^p\right]} - (\sigma^y + Cp) = 0$$

Thus, initial stress states lying on the initial yield surface can be set for several values of σ_{11} and by enforcing $f(\boldsymbol{\sigma}) = 0$ through the choice of σ_{12}, namely:

$$\sigma_{12} = \pm\sqrt{\frac{(\sigma^y + Cp)^2 - (\sigma_{11}^2 + \sigma_{22}^2)(\nu^2 - \nu + 1) - \sigma_{11}\sigma_{22}(2\nu^2 - 2\nu - 1) + E\varepsilon_{33}^p\left[(\sigma_{11} + \sigma_{22})(1 - 2\nu) + E\varepsilon_{33}^p\right]}{3}} \quad (57)$$

for $p = 0$ and $\varepsilon_{33}^p = 0$. As previously, the initial values of σ_{11} form a symmetrical set with respect to zero. The numerical integration in then made with σ_{12} used as a driving parameter and again by considering the semi-space $\sigma_{12} > 0$ for the initial stress state.

6.3.1. Fast waves

The loading paths followed in a fast wave are first looked at by decreasing the shear stress component σ_{12}. Analogously to what has been done before, figure 12 shows the paths in two planes of the stress space, while the same paths are depicted in the deviatoric plane in figure 13. Once again, the evolution of the characteristic speed associated with fast waves is depicted in the figures by means of a color gradient, which confirms that the simple wave solution is valid.

First, the curves depicted in figure 12 show the symmetry of σ_{12} with respect to the σ_{12}-axis. Second, as for the plane stress situation, the loading paths followed inside fast waves are smooth. Notice however that the curves do not overlap in the $(\sigma_{11}, \sigma_{12})$ plane as it was the case before. At last, it appears that all the paths tend to the σ_{11}-axis which, as predicted by the analytical results in table 3, would lead to curves that follow the axis.

On the other hand, the paths projected in the deviatoric plane show once again that the von-Mises circle is traced by the integral curves. Moreover, opposite signs for the initial values of σ_{11} lead to curves that are symmetric with

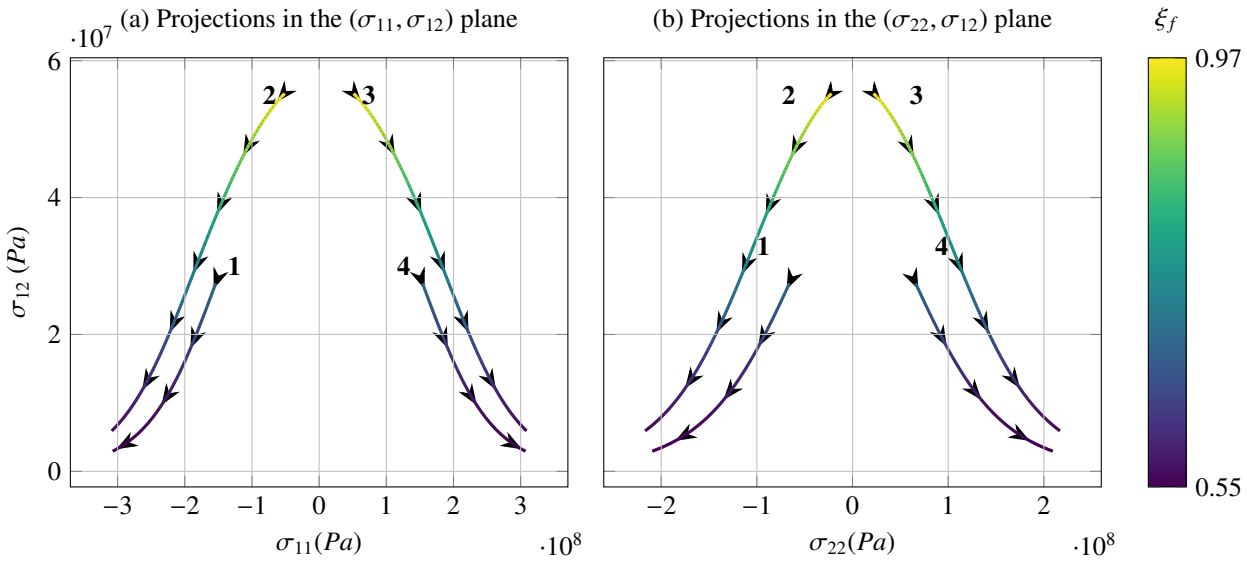

Figure 12: Loading paths through a fast simple wave under plane strain conditions in the stress planes $(\sigma_{11}, \sigma_{12})$ and $(\sigma_{22}, \sigma_{12})$ for several starting points lying on the initial yield surface.

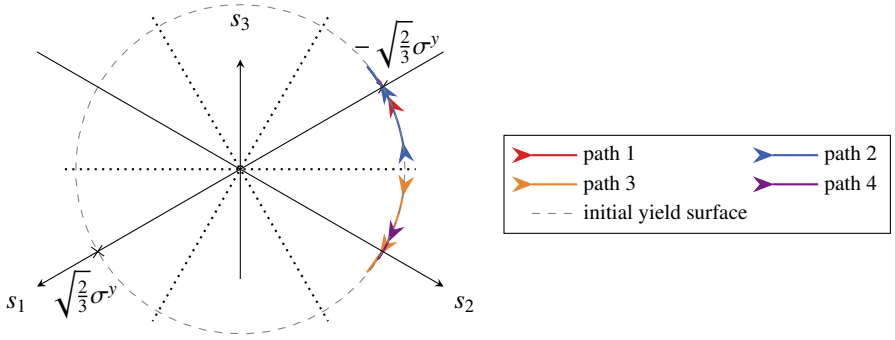

Figure 13: Loading paths through a fast simple wave under plane strain conditions in the deviatoric plane for several starting points lying on the initial yield surface.

respect to the horizontal axis. Unlike the plane stress case, for which the fast wave loading paths reach a direction of pure shear in the deviatoric plane, the curves in figure 13 all exhibit a cusp so that the paths tend to a direction of pure tension/compression after crossing it. Increasing the hardening modulus to $C = 10^{10}\ Pa$ enables emphasizing this phenomenon, as depicted in figure 14. After being restricted to the initial yield surface beyond a direction of pure tension/compression, the paths all branch off towards the latter. It then seems that once this direction is achieved, the plastic flow is radial. However, since no singular behavior is seen in the stress space in figure 12, it is difficult to identify the stress states that are responsible for that response.

6.3.2. Slow waves

We finish this section by considering the loading paths in a slow wave under plane strain conditions. The integration of the corresponding ODEs is performed by using σ_{12} as a driving parameter.

First, figure 15 shows two projections of the paths in the stress space. Analogously to plane stress problems, the curves projected in the $(\sigma_{11}, \sigma_{12})$ plane can be pretty well approximated with straight lines. Moreover, both projections

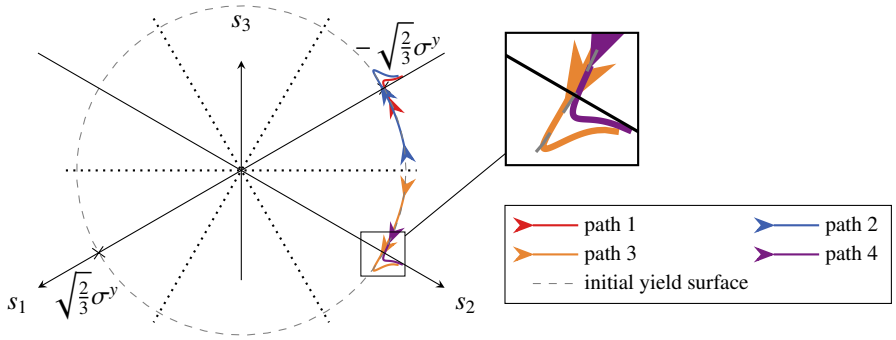

Figure 14: Loading paths through a fast simple wave under plane strain conditions in the deviatoric plane for several starting points lying on the yield surface with an increased hardening modulus.

emphasize some symmetry with respect to the σ_{12}-axis. In addition, rough slope changes occur in the $(\sigma_{22}, \sigma_{12})$ plane (see the paths 3 and 4 in figure 15b). Once again, these inflections are due to the reaching of the maximum shear stress

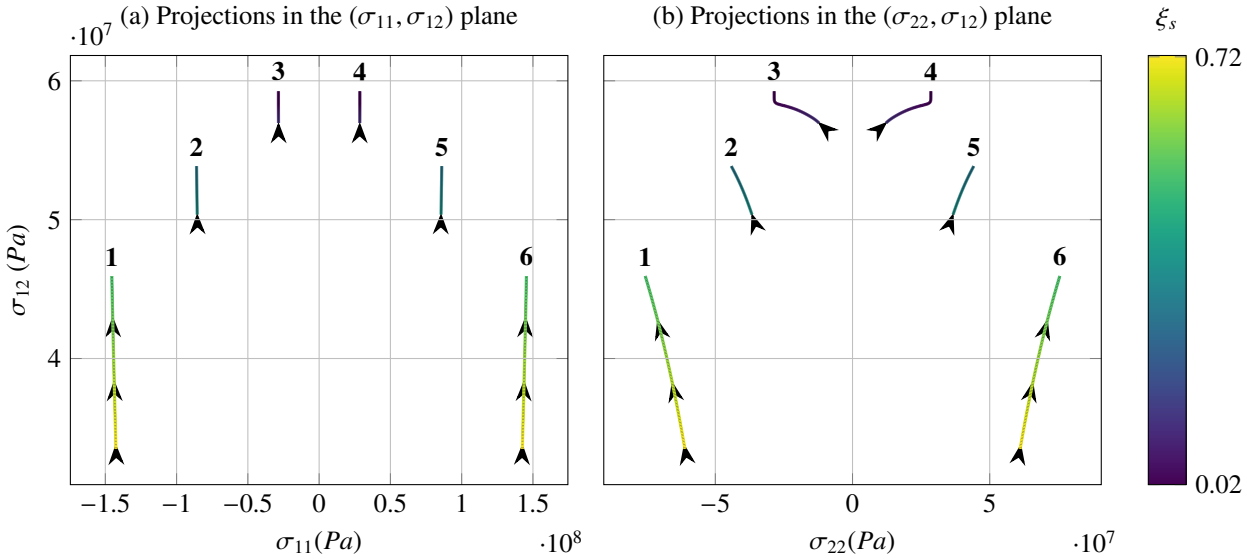

Figure 15: Loading paths through a slow simple wave under plane strain conditions in the stress planes $(\sigma_{11}, \sigma_{12})$ and $(\sigma_{22}, \sigma_{12})$for different starting points on the initial yield surface.

σ_{12} for a given state $(\sigma_{11}, \sigma_{33})$ on the current yield surface. Indeed, requiring that the partial derivative of equation (57) with respect to σ_{22} vanishes, one writes:

$$2\sigma_{22} - \bar{\sigma} = 0 \tag{58}$$

$$\text{with } \bar{\sigma} = \frac{\sigma_{11}(2\nu^2 - 2\nu - 1) + E\varepsilon^p_{33}(1 - 2\nu)}{\nu - \nu^2 - 1}$$

Figure 16 shows the evolution of the ratio $2\sigma_{22}/\bar{\sigma}$ with respect to σ_{12} and σ_{22} for all the loading paths, though particular attention must be paid to the paths 3 and 4. To begin with, the plotting of $2\sigma_{22}/\bar{\sigma}$ as a function of σ_{12} in figure 16a confirms the symmetry observed above since symmetrical initial values with respect to zero yield overlapping curves. Next, it can be seen that the ratio tends to unity for the paths 3 and 4 while it is not the case for the others. As soon

as that value is reached, $2\sigma_{22}/\bar{\sigma}$ stop varying even though σ_{12} continues increasing. Looking at figure 16b, in which the evolution of the ratio with respect to σ_{22} is depicted, one sees that the limit $2\sigma_{22}/\bar{\sigma} = 1$ also corresponds to an upper bound for σ_{22}. Indeed, the curves corresponding to paths 3 and 4 are monotone up to the *maximum-shear-stress* condition (58) is fulfilled. After this, all the points overlap so that both $2\sigma_{22}/\bar{\sigma}$ and σ_{22} are constant. This discussion once again highlights the shearing nature of slow waves.

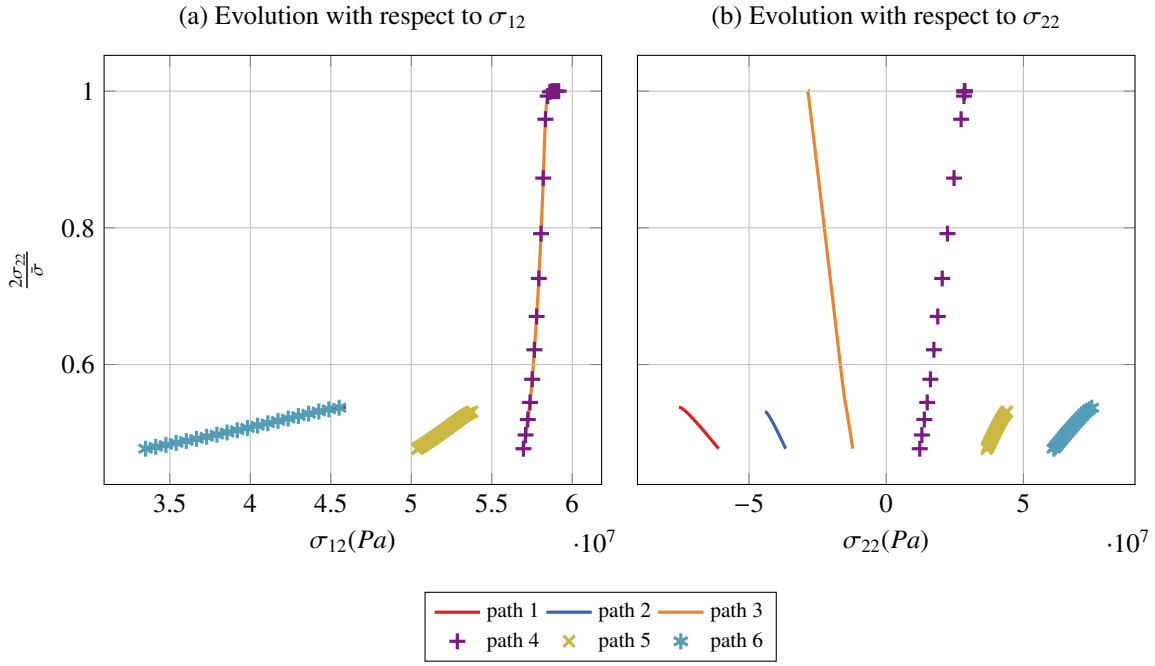

Figure 16: Evolution of the ratio $\frac{2\sigma_{22}}{\bar{\sigma}}$ along the loading paths through a slow wave under plane strain conditions.

We now focus on the projections of the loading paths in the deviatoric plane in figure 17. The projections of the stress paths in the deviatoric plane in figure 17a is supplemented with the evolution of the ratio $\frac{2\sigma_{22}}{\bar{\sigma}}$ with respect to the Lode parameter in figure 17b. Despite the non-zero out-of-plane stress component that leads to loading paths taking values in the whole space $(\sigma_1, \sigma_2, \sigma_3)$, the paths are not more complex than for plane stress. Indeed, the paths are much simpler since they all follow the initial yield surface up to a direction of pure shear, and next follow the radial direction. On the other hand, figure 17b enables to better distinguish the curves that are superimposed in figure 17a. It also highlights that the slope breaks which are observed in the deviatoric plane do not correspond to the maximum shear stress condition (58). As a matter of fact, the loading paths 2, 3, 4 and 5 become radial for $\cos(3\Theta) \equiv 0$, which occurs before the value $\frac{2\sigma_{22}}{\bar{\sigma}} = 1$ is achieved.

As for the results presented for fast waves, increasing the hardening parameter to $C = 10^{10} Pa$ allows smoothing the curves. Furthermore, considering a higher hardening modulus enables to integrate the loading paths further without numerical issues related to a growing characteristic speed. Thus, figure 18 shows the stress paths resulting from the integration driven by σ_{12} as well as the evolution of condition (58) with respect to the Lode parameter. It can then be seen in figure 18a that the loading paths are no longer restricted to the initial yield surface but start moving away from it quasi-instantaneously. Moreover, all the curves converge to the direction of pure shear. The main difference with the results depicted in figure 17 arises in figure 18b. The *maximum-shear-stress* condition (58) is now satisfied at the very end of the numerical integration, once the direction of pure shear is reached in all the loading paths. Therefore, the results of figure 17b must be considered carefully depending on the value of the hardening modulus. Similar conclusions have been also drawn for plane stress problems in section 6.2.

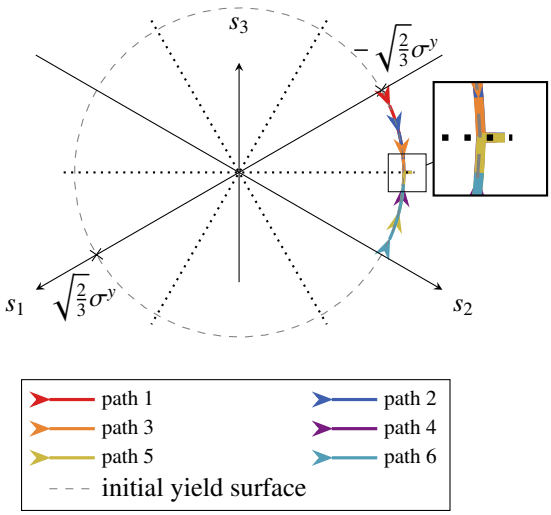

(a) Loading paths in the deviatoric plane

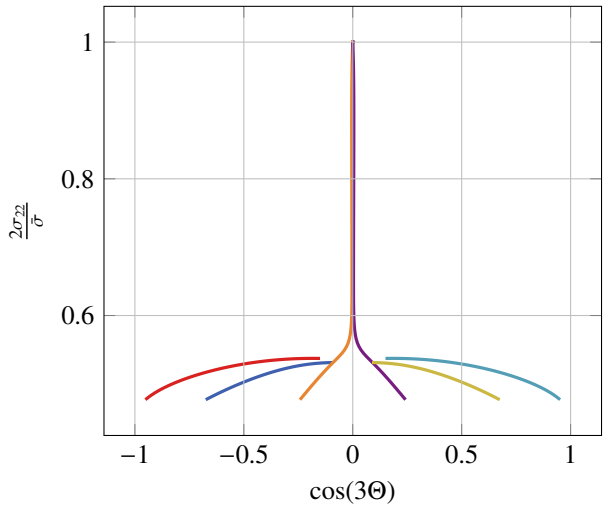

(b) Evolution of $\frac{2\sigma_{22}}{\bar{\sigma}}$ with respect to the Lode parameter

Figure 17: Study of the loading paths through slow simple waves under plane strain conditions: (a) Loading path in the deviatoric plane; (b) Evolution of the ratio $\frac{2\sigma_{22}}{\bar{\sigma}}$ with respect to the Lode parameter along the loading path. The legend stands for both figures.

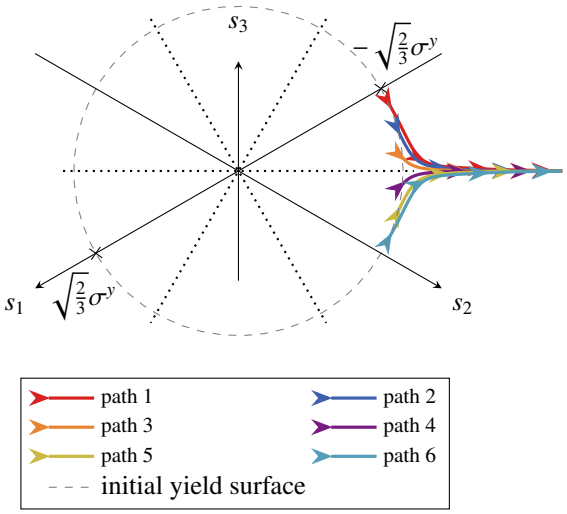

(a) Loading paths in the deviatoric plane

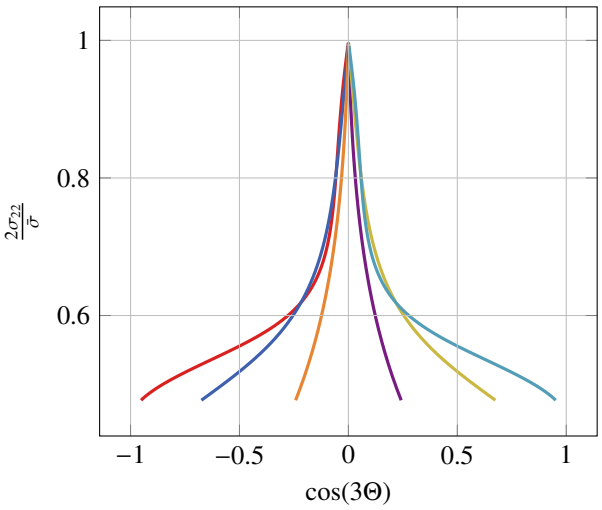

(b) Evolution of $\frac{2\sigma_{22}}{\bar{\sigma}}$ with respect to the Lode parameter

Figure 18: Study of the loading paths through slow simple waves in the principal deviatoric stress space with an increased hardening modulus.

7. Conclusion

7.1. Summary of the important contributions

In this paper, the characteristic structure of the solution of hyperbolic problems in elastic-plastic solids in two space dimensions has been highlighted. First, a thermodynamically-consistent formulation leading to the writing of a hyperbolic system involving the fourth-order elastic-plastic stiffness tensor as been proposed. The aforementioned

tensor can be easily specialized to plane stress and plane strain problems in such a way that the quasi-linear form derived provides a generic framework for the study of all mechanical problems in two space dimensions.

Second, the characteristic analysis of the hyperbolic plane strain and plane stress problems has been carried out. As already emphasized for simpler two-dimensional problems in prior works [3, 4] the solutions involve slow and fast simple waves. The characteristic equations governing the evolution of the system inside the simple waves have then been derived as a set of ODEs by applying the method of characteristics.

Third, some mathematical properties of these characteristic equations have been highlighted for plane strain and plane stress, despite the complexity of the equations. As an interesting result of this work, it has been shown that the loading paths followed inside slow and fast waves are perpendicular in the stress space. Although this feature has been already emphasized in [8] for a combined longitudinal and torsional loading, the property is in fact due to the symmetry of the acoustic tensor and is therefore valid for all two-dimensional problems.

At last, to overcome the mathematical complexity of the characteristic equations, numerical investigations have been proposed. The loading paths depicted in the stress space or in the deviatoric plane then enable the identification of symmetry properties that are not proofed mathematically. Moreover, the integral curves holding inside fast waves are restricted to the initial yield surface for both plane stress and plane strain situations. In the former case, the paths end as soon as a direction of pure shear is reached in the deviatoric plane, whereas in the latter one, the paths appears to be radial once a direction of pure tension/compression is achieved. On the other hand, the loading through the simple waves exhibit rough changes regardless of the kinematic considered for low hardening moduli (*i.e.* $C = \mathcal{O}(10^8)$). It has moreover been shown numerically that this inflection corresponds, for plane stress, to the reaching of the maximum shear stress on the current yield surface for a given longitudinal stress. For plane strain, a similar response is also seen but before the *maximum-shear-stress* condition is achieved. Nevertheless, increasing the hardening modulus leads to loading paths whose direction changes before the *maximum-shear-stress* condition is achieved for plane stress, and which reach a direction of pure shear at the same time as the maximum shear stress.

7.2. Concluding remarks

The results of the present paper allow a better understanding of the physical response of linearly hardening elastic-plastic solids to dynamic loadings. However, the singularities that have been highlighted numerically still need to be identified mathematically. Notice that kinematic hardening should yield identical results for the monotonic loadings considered here, but would greatly influence the response for unloading or reverse plastic loading. These waves must also be the object of an analysis for two-dimensional problems in order to construct the solution of the Riemann problem. As a more long-term perspective, the elementary loading paths studied here could be used in order to enrich numerical methods based on the use of Riemann solvers. In fact, following the idea of Lin and Ballman [21], a numerical procedure that accounts for both elastic and plastic characteristics can be developed in order to improve the tracking of waves in elastic-plastic solids.

References

[1] G. Taylor, The plastic wave in a wire extended by an impact load, Tech. Rep. R.C. 329, British official report (1942).

[2] T. von Kármán, On the propagation of plastic deformation in solids, Tech. rep., National Defense Research Commitee (1942).

[3] K. Rakhmatulin, On the propagation of elastic-plastic waves owing to combined loading, Journal of Applied Mathematics and Mechanics 22 (6) (1958) 1079 – 1088. doi:https://doi.org/10.1016/0021-8928(58)90034-0.

[4] N. Cristescu, On the propagation of elasto-plastic waves for combined stresses, Journal of Applied Mathematics and Mechanics 23 (6) (1959) 1605 – 1612. doi:https://doi.org/10.1016/0021-8928(59)90016-4.

[5] J. Mandel, Ondes plastiques dans un milieu indéfini à trois dimensions, J. Mécanique 1 (1) (1962) 3–30.

[6] R. Hill, Acceleration waves in solids, Journal of the Mechanics and Physics of Solids 10 (1) (1962) 1 – 16. doi:https://doi.org/10.1016/0022-5096(62)90024-8.

[7] H. Bleich, I. Nelson, Plane waves in an elastic-plastic half-space due to combined surface pressure and shear, Journal of Applied Mechanics 33 (1) (1966) 149–158.

[8] R. Clifton, An Analysis of Combined Longitudinal and Torsional Plastic Waves in a Thin-Walled Tube, Proc. 5th U. S. National Congress of Appl. Mech. (1966) 465 – 480.

[9] J. Lipkin, R. J. Clifton, An experimental study of combined longitudinal and torsional plastic waves in a thin-walled tube, in: M. Hetényi, W. G. Vincenti (Eds.), Applied Mechanics, Springer Berlin Heidelberg, Berlin, Heidelberg, 1969, pp. 292–304.

[10] J. Lipkin, R. Clifton, Plastic waves of combined stresses due to longitudinal impact of a pretorqued tube–part 1: Experimental results, Journal of Applied Mechanics 37 (4) (1970) 1107–1112.

[11] T. Ting, N. Nan, Plane waves due to combined compressive and shear stresses in a half space, Journal of Applied Mechanics 36 (2) (1968) 189–197.
[12] T. Ting, Elastic-plastic boundaries in plane and cylindrical wave propagation of combined stresses, Tech. rep., Department of Applied Mechanics, Stanford University (1969).
[13] W. K. Nowacki, Stress waves in non-elastic solids, Elsevier, 2018.
[14] M. Rice, R. McQueen, J. Walsh, Compression of solids by strong shock waves**work done under auspices of the u. s. atomic energy commission., in: F. Seitz, D. Turnbull (Eds.), Advances in Research and Applications, Vol. 6 of Solid State Physics, Academic Press, 1958, pp. 1 – 63. doi:https://doi.org/10.1016/S0081-1947(08)60724-9.
[15] L. W. Morland, The propagation of plane irrotational waves through an elastoplastic medium, Philosophical Transactions of the Royal Society of London. Series A, Mathematical and Physical Sciences 251 (997) (1959) 341–383.
[16] P. Germain, E. Lee, On shock waves in elastic-plastic solids, Journal of the Mechanics and Physics of Solids 21 (6) (1973) 359–382.
[17] J. Dequiedt, C. Stolz, Propagation of a shock discontinuity in an elasto-plastic material: constitutive relations, Arch. Mech. 56 (5) (2004) 391–410.
[18] J. Mandel, Ondes de choc longitudinal dans un milieu élastoplastique, Mech. Res. Comm. 5 (6) (1978) 353–359.
[19] L. Wang, Foundations of stress waves, Elsevier, 2011.
[20] S. K. Godunov, Finite difference method for numerical computation of discontinuous solutions of the equations of fluid dynamics, Matematicheskii Sbornik 47(89) (3) (1959) 271–306.
[21] X. Lin, J. Ballmann, A riemann solver and a second-order godunov method for elastic-plastic wave propagation in solids, International Journal of Impact Engineering 13 (3) (1993) 463 – 478.
[22] Z. Mróz, B. Raniecki, On the uniqueness problem in coupled thermoplasticity, International Journal of Engineering Science 14 (2) (1976) 211 – 221. doi:https://doi.org/10.1016/0020-7225(76)90090-2.
[23] J. Mandel, L. Brun, Ordinary waves in inviscid plastic media, in: Mechanical waves in solids, Vol. 222, Springer, 1975, pp. 157–220.
[24] R. J. Leveque, Finite volume methods for hyperbolic problems, Cambridge university press, 2002.
[25] E. F. Toro, Riemann solvers and numerical methods for fluid dynamics: a practical introduction, Springer Science & Business Media, 2013.
[26] R. J. Clifton, Analysis of dynamic deformation of elastic-plastic solids under condition of plane strain, Ph.D. thesis, Inst. Techn. Pittsburg (1963).
[27] B. J. Plohr, D. H. Sharp, A conservative eulerian formulation of the equations for elastic flow, Advances in Applied Mathematics 9 (4) (1988) 481 – 499.
[28] J. Bonet, A. J. Gil, C. H. Lee, M. Aguirre, R. Ortigosa, A first order hyperbolic framework for large strain computational solid dynamics. part i: Total lagrangian isothermal elasticity, Computer Methods in Applied Mechanics and Engineering 283 (2015) 689 – 732. doi:https://doi.org/10.1016/j.cma.2014.09.024.
[29] J. Trangenstein, P. Colella, A higher-order godunov method for modeling finite deformation in elastic-plastic solids, Communications on Pure and Applied Mathematics 44 (1991) 41–100.
[30] B. Halphen, Q. S. Nguyen, Sur les matériaux standard généralisés, Journal de mécanique 14 (1975) 39–63.
[31] J. C. Simo, T. J. Hughes, Computational inelasticity, Vol. 7, Springer Science & Business Media, 2006.
[32] J. E. Marsden, T. J. Hughes, Mathematical foundations of elasticity, Courier corporation, 1994.
[33] G. Kluth, Analyse mathématique et numérique de systèmes hyperélastiques et introduction de la plasticité, Ph.D. thesis, Université Paris 6 (2008).
[34] P. J. Mandel, Thermodynamique et ondes dans les milieux viscoplastiques, Journal of Mechanics Physics of Solids 17 (3) (1969) 125–140. doi:10.1016/0022-5096(69)90027-1.
[35] R. Courant, D. Hilbert, Methods of mathematical physics [Methoden der mathematischen Physik, engl.] 1, CUP Archive, 1965.
[36] W. Lode, Versuche über den einfluß der mittleren hauptspannung auf das fließen der metalle eisen, kupfer und nickel, Zeitschrift für Physik 36 (11) (1926) 913–939. doi:10.1007/BF01400222.